https://doi.org/10.5194/egusphere-2026-3092
Preprint. Discussion started: 18 June 2026

Turbulence structure of dusty cirrus and its relation to atmospheric conditions: A characterization using cloud-radar measurements and reanalysis data

Lukas Pieper[1], Patric Seifert[1], Hannes Griesche[1], Albert Ansmann[1], George McCosh[1], Florian Ewald[2], and Stefan Kneifel[3]

[1]Leibniz Institute for Tropospheric Research (TROPOS), Leipzig
[2]Institute of Atmospheric Physics, German Aerospace Center (DLR), Oberpfaffenhofen
[3]Institute for Meteorology, Ludwig-Maximilians-University (LMU), Munich

Correspondence: Lukas Pieper (pieper@tropos.de)

Abstract. Several times per year, Saharan dust intrusions reach central Europe and lead to the so-called dusty cirrus phenomenon. Numerical weather prediction models often struggle to reproduce these dusty cirrus clouds . This study presents the first characterization of the atmospheric conditions associated with dusty cirrus formation, using long-term, height-resolved observations from ground-based remote sensing. Continuous measurements from the Cloudnet station at Schneefernerhaus throughout the year 2022 were evaluated using cloud-radar measurements to explore the turbulent structure of cirrus clouds in the presence of Saharan dust. Observations were compared with simulated dust concentrations from the EAC4 (European Centre for Medium range Weather Forecasts (ECMWF) Atmospheric Composition 4) Global Reanalysis product provided by the Copernicus Atmosphere Monitoring Service (CAMS) to investigate links between dust and turbulence in cirrus clouds. This study further explores the atmospheric mechanisms that lead to dusty cirrus formation including the influence of wind shear on the observed turbulence structure. The results reveal a clear link between elevated dust concentrations and increased turbulence. No cases of strong turbulence in the absence of elevated dust concentrations, or vice versa were observed. Increased turbulence and the associated higher frequency of vertical updrafts, may promote heterogeneous ice nucleation in dusty cirrus clouds. Wind shear does not seem to be a significant factor influencing the observed turbulence. Further analysis of the atmospheric conditions observed around dusty cirrus clouds suggest that current theories might not fully capture the processes involved in this phenomenon.

1 Introduction

Clouds and aerosol particles play a key role in modulating the energy budget of our planet by reflecting incoming shortwave radiation and trapping outgoing longwave radiations. In general, radiative effects of cirrus clouds are suspected to cause significant climate forcing (Intergovernmental Panel On Climate Change (IPCC), 2023). Aerosol-cloud interactions (ACI) introduce additional complexity, as they can change cloud properties such as the cloud life time and the cloud albedo (Albrecht, 1989; Twomey, 1977). Specific aerosol particles can serve as cloud condensation nuclei (CCN) and/or ice-nucleating particles (INPs),

https://doi.org/10.5194/egusphere-2026-3092
Preprint. Discussion started: 18 June 2026

influencing droplet and ice formation pathways, respectively (Pruppacher and Klett, 1997). Ice formation in cirrus clouds can occur either homogeneously, by spontaneous freezing of supercooled solution droplets or heterogeneously, where ice formation is initiated by INPs (Hoose and Möhler, 2012; Ansmann et al., 2025b; Kärcher, 2022). Studies have demonstrated that cirrus cloud lifetime and radiative properties are linked through the primary ice formation pathway (Kuebbeler et al., 2014; Penner et al., 2018).

Due to its complexity, significant knowledge gaps remain regarding the relationship between aerosol particles and cirrus cloud microphysical properties (Kärcher et al., 2022). In a review paper about the response of cirrus clouds to anthropogenic activities, Kärcher (2017) defined two critical factors that constrain the ability of climate models to accurately simulate cirrus formation: the correct representation of small-scale variabilities in atmospheric dynamics and the parameterizations of heterogeneous ice formation. According to the author, uncertainties in these processes and their influence on cirrus formation must be addressed before the anthropogenic impact can be accurately estimated. In recent years, several studies have been published, which explore the effects of aerosol particles on cirrus clouds. Kärcher (2018) demonstrated, how soot particles emitted by aircraft contribute to the formation of cirrus clouds and thus induce a warming effect on the climate system. Based on radar and lidar observations from the MOSAiC (Multidisciplinary drifting Observatory for the Study of Arctic Climate) expedition in the Arctic in 2019 and 2020, Ansmann et al. (2025a) found that high concentrations of aged Siberian wildfire smoke significantly influenced heterogeneous cirrus formation. In a complementary study, Ansmann et al. (2025b) simulated the adiabatic ascent of a smoke-laden air parcel originating from the top of the cirrus cloud. Using meteorological input parameters from the MOSAiC observations, they tested whether the observed ice crystal number concentration (ICNC) could be reproduced solely through heterogeneous nucleation. Their results showed that low-amplitude updrafts of $100\tilde{}120\,\mathrm{m}$ associated with gravity waves were generally sufficient to initiate heterogeneous ice nucleation under the observed high aerosol load. As Saharan dust has been identified as a highly efficient INP (Hoose and Möhler, 2012; Koehler et al., 2010; Seifert et al., 2010) and can initiate heterogeneous ice formation at temperatures below -15°C and at ice saturation ratios as low as $1.15\tilde{}1.25$ (Ansmann et al., 2019; Hoose and Möhler, 2012), this suggests, that the small-scale turbulence associated with dusty cirrus, in combination with an enhanced availability of dust may effectively trigger cirrus formation.

Several times per year, an extended cirrus cloud deck coinciding with a Saharan dust plume can be observed over Europe (Seifert et al., 2023). This so-called dusty cirrus phenomenon provides a great example of aerosol-cloud interaction effects on cirrus formation and their incomplete representation in current models. Fromm et al. (2016) identified dust-infused baroclinic storms (DIBS) as the synoptic-scale events responsible for dusty cirrus formation. These extra-tropical cyclones extend southward over the Sahara desert and generate high surface windspeeds capable of entraining dust from arid regions of North Africa. Similar mechanisms were observed over desert regions of Mongolia and China. Warm conveyor belts (WCB) at the frontal regions of these systems subsequently transport the dust masses northward and into the upper troposphere. Kollath (2010); Seifert et al. (2023) and Fromm et al. (2016) identify the cellular structure that can be observed in satellite images as one of the most prominent characteristics of the resulting dusty cirrus cloud decks.

Different mechanisms have been proposed that can lead to the formation of such a dusty cirrus phenomenon. In a technical report for EUMETSAT (European Organisation for the Exploitation of Meteorological Satellites) Kollath (2010) proposed

https://doi.org/10.5194/egusphere-2026-3092
Preprint. Discussion started: 18 June 2026

nighttime radiative cooling as the key driver of dusty cirrus formation. He attributes the convective structure to longwave radiative cooling at the top of the cirrus cloud layer during the night, which leads to a destabilization of the cloud layer and thus creates small-scale convection within the cloud. He further hypothesizes that increased absorption of short-wave radiation during daytime leads to a more stable stratification, which in turn would dissolve the turbulent structure of the dusty cirrus over the course of the day. This theory is largely based on 2-D satellite images. When investigating the relationship between cirrus clouds and radiation in a modeling study, Fusina and Spichtinger (2010) concluded, that in case of supersaturated air layers, radiative cooling can lead to destabilization and subsequent ice formation. Latent heat release through the initial cirrus formation can then produce small-scale turbulence with updraft velocities of up to $1 - 2\,\mathrm{m\,s^{-1}}$. Seifert et al. (2023) proposed that the cirrus formation they investigated was initiated at the interface of a dry dusty air layer and a supersaturated dust-free air layer above. Lofting by gravity waves or shear-induced turbulence led to the initial cirrus formation via heterogeneous ice nucleation. Subsequent longwave radiative cooling at the top of the initial cirrus caused destabilization and convective overturning within the cirrus layer. Turbulent mixing at the interface entrained dust aerosol into the moist layer, thickening the initial cirrus cloud. Based on this theory, the authors have developed a dusty cirrus parameterization within the ICOsahedral Nonhydrostatic model – Aerosol and Trace Gases (ICON – ART). The scheme requires three primary conditions to enable dusty cirrus formation: (1) neutral atmospheric stratification that allows for vertical mixing, (2) elevated dust concentrations, and (3) relative humidity levels sufficient to initiate subscale nucleation processes. In contrast to the study of Seifert et al. (2023), Ansmann et al. (2019) found that cirrus usually formed within the dust layer and not at the interface of two layers (which will be referred to as in-layer formation).

To assess the proposed dusty cirrus formation mechanisms, it is necessary to characterize the general atmospheric conditions leading to the formation of dusty cirrus, as well as dusty cirrus turbulence. Seifert et al. (2023) proposed that wind shear or gravity waves could be responsible for the initial lofting required for heterogeneous nucleation. According to a study by Podglajen et al. (2016), the upper troposphere-lower stratosphere (UTLS) in which cirrus formation preferentially takes place is frequently affected by low amplitude perturbations primarily caused by interfering gravity waves. Using super pressure ballon measurements, they managed to quantify wave-induced fluctuations in temperature and vertical velocity along the trajectories of air parcels. Additionally, small-scale lofting has been shown to initiate heterogeneous nucleation through changes in temperature and supersaturation (Ansmann et al., 2025b; Spichtinger, 2014; Kärcher et al., 2024), and thereby might significantly influence cirrus formation.

Seifert et al. (2023) and Weger et al. (2018) showed that direct radiative effects of mineral dust in the atmosphere are negligible in the presence of dusty cirrus while its effect on aerosol-cloud interactions (ACI) via heterogeneous nucleation remains important. Seifert et al. (2023) even referred to dusty cirrus as the “dominant aerosol–cloud–radiative effect of mineral dust over Europe”. Operational numerical weather prediction (NWP) models still struggle to accurately simulate dusty cirrus events, indicating deficiencies in ACI parameterizations (Griesche, 2016; Seifert et al., 2023; Weger et al., 2018). Seifert et al. (2023) and Weger et al. (2018) both show that even state-of-the-art ACI schemes, including aerosol emissions and transport are unable to reproduce the observed cloud cover during dust events. Weger et al. (2018) attribute to uncertainties regarding heterogeneous ice nucleation as well as to an underestimation of specific humidity at cirrus altitudes. Most current schemes

https://doi.org/10.5194/egusphere-2026-3092
Preprint. Discussion started: 18 June 2026

rely on time-independent parameterizations of heterogeneous nucleation. These approaches do not adequately capture the coupling between ice formation, evolving environmental conditions (e.g. relative humidity and temperature changes), and the ice-nucleating particle (INP) reservoir as they assume instantaneous activation of all available INP. Ansmann et al. (2025b) propose a time-dependent framework based on classical nucleation theory as a more physically consistent representation of heterogeneous nucleation processes. In addition, Seifert et al. (2023) argue that typical model resolutions are too coarse to represent the sub-grid processes that initiate dusty cirrus formation. They introduced a sub-grid parametrization aimed at improving the simulation of these processes.

So far, the relationship between dust and turbulence in cirrus clouds has not been investigated. The objective of this study is to investigate the turbulent structure and the surrounding atmospheric conditions of dusty cirrus cloud decks using ground-based height-resolved remote sensing. The analysis is based on a year-long dataset from the Cloudnet station at Schneefernerhaus for 2022. Dust concentrations from the EAC4 global reanalysis of the Copernicus Atmosphere Monitoring Service (CAMS) are used to distinguish dusty from non-dusty cirrus cloud decks. This study provides a first characterization of the dusty cirrus phenomenon using ground-based height-resolved remote sensing and establishes a basis for future investigation of cirrus microphysics under enhanced aerosol loads.

The paper is structured as follows: The datasets and methods used in this study are described in Sect 2. The results are presented in Sect. 3, beginning with a statistical evaluation of the relationship between dust and cirrus cloud turbulence (Sect. 3.1), followed by selected case studies (Sect. 3.2). Finally, Section 4 provides a summary of the main findings and a discussion of their implications.

2 Data and Methods

This section introduces the overall analysis workflow (Sect 2.1), as well as observational networks and datasets (Sects. 2.2 and 2.3) used in this study. It also describes the methods applied to retrieve information about dust concentration (Sect. 2.4), turbulence (Sect. 2.5) and relevant atmospheric parameters (Sect. 2.6).

2.1 Analysis workflow

Figure 1 illustrates the workflow used to investigate the relationships between dust load, turbulence and other meteorological conditions associated with dusty cirrus. The eddy dissipation rate, relative humidity w.r.t. ice , temperature, and vertical wind shear were retrieved from Cloudnet observations and model output. Dust mixing ratios from the Copernicus Atmosphere Monitoring Service (CAMS) were used to derive the total dust concentration. The cirrus level was defined as the atmospheric region above the altitude where air temperatures fall below the homogeneous freezing threshold of $-38\,°C$, where the presence of supercooled liquid water can be excluded. The dust load was integrated from this altitude upwards, and eddy dissipation rate (EDR) values from below this level were not considered in the analysis. A yearly timeline of the mean dust load and EDR, and normalized cloud pixel count was created to identify periods characterized by increased dust load and turbulence, as well as sufficiently high cloud cover to ensure statistically meaningful information content. Cloud pixel were defined as all pixel

https://doi.org/10.5194/egusphere-2026-3092
Preprint. Discussion started: 18 June 2026

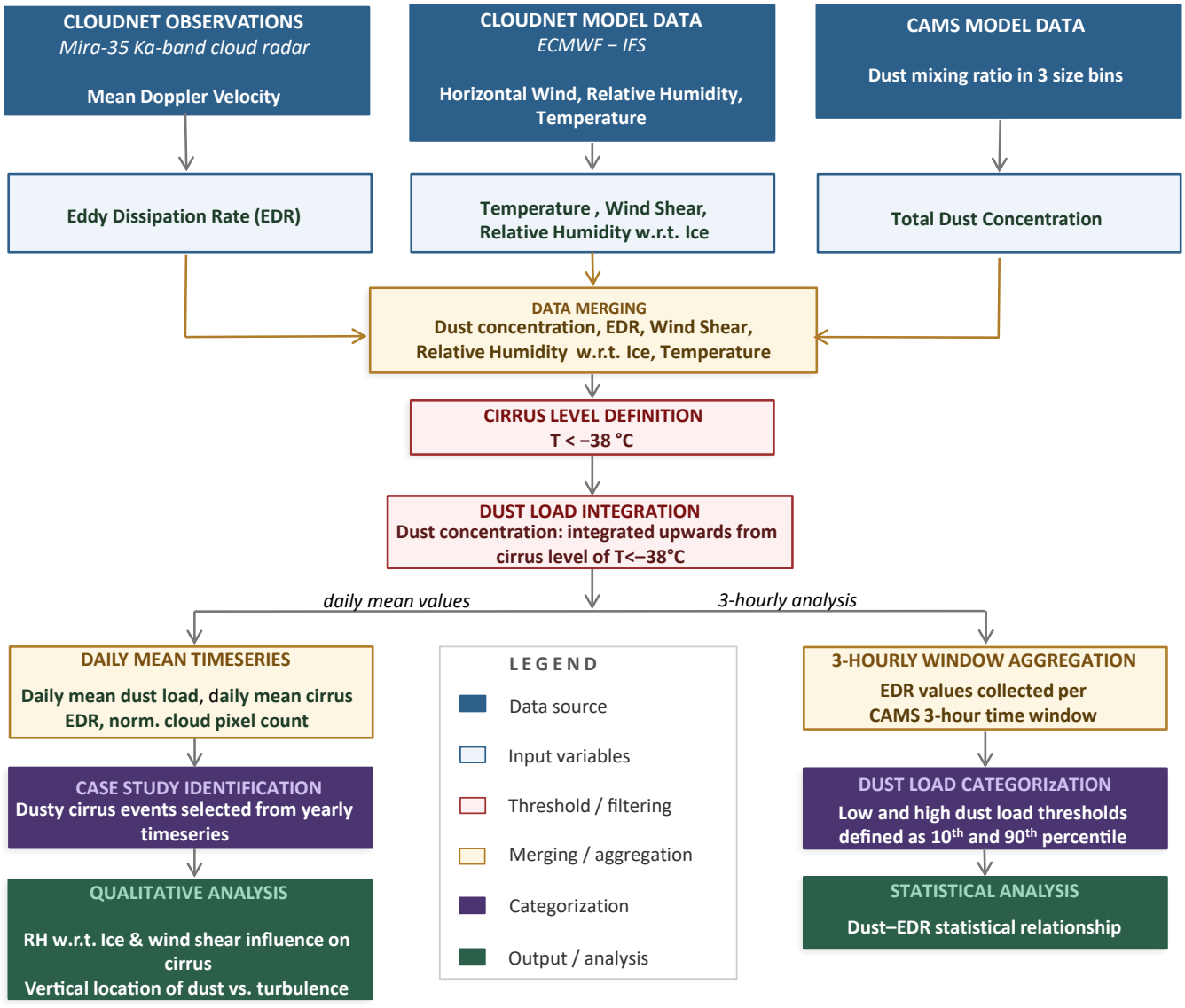

Figure 1. Analysis workflow illustrating the datasets, variables, and processing steps used to investigate the relationship between dust load, turbulence, wind shear, and relative humidity (RH) w.r.t. ice at cirrus level.

https://doi.org/10.5194/egusphere-2026-3092
Preprint. Discussion started: 18 June 2026

where an EDR value can be retrieved. These cases were used to investigate the influence of relative humidity w.r.t. ice and vertical wind shear on the cirrus and to examine the relationship between cirrus turbulence and the presence of dust aerosol. As the CAMS dataset is provided at a 3-hour temporal resolution, EDR values were grouped within corresponding 3-hour time windows around each dust load in order to explore the statistical relationship between dust load and cirrus turbulence. Thresholds for high dust load and dust-free conditions were defined using the 90th and 10th percentiles of the modeled dust load distribution, respectively. EDR values associated with high- and low-dust conditions were then compared using histograms of their respective EDR distributions. In addition, all EDR observations were further split into 20 dust load bins to examine the dependence of cirrus turbulence on dust concentration. The datasets and processing steps are described in more detail in the following sections. The statistical analyses at daily and 3-hour resolution are presented in the results section (Sec. 3).

2.2 ACTRIS Cloudnet dataset

Cloudnet, as part of ACTRIS (Aerosol, Clouds and Trace Gases Research Infrastructure), is an international network of ground-based remote sensing sites operated by different European institutes (Tukiainen et al., 2020; Illingworth et al., 2007). Standard equipment at all Cloudnet sites include a Doppler cloud radar, a ceilometer (lidar), and a microwave radiometer, usually operated 24/7. Based on the synergistic approach of Cloudnet, ice and liquid cloud microphysical properties can be derived using existing approaches (e.g., Frisch et al. (2002), Hogan et al. (2006), Griesche et al. (2020), Kneifel and Moisseev (2020)).

The Cloudnet station at Schneefernerhaus was selected because it fulfills several important criteria. First, it provides sufficient vertical and temporal resolution for detailed cloud observations. Second, the data availability at Schneefernerhaus is comparably high, as many Saharan dust events do not reach much further north, making this site particularly suitable for studying dusty cirrus clouds. While other Cloudnet stations (e.g., Jülich, Leipzig, or Lindenberg) provide a slightly better temporal resolution and longer continous measurements, they observe fewer Saharan dust events. The local topography at Schneefernerhaus might cause some orographic effects. However, considering the reasons stated above, Schneefernerhaus is still a valuable site to study dusty cirrus effects. Further discussions related to orographic effects are presented in the conclusions section.

The Environmental Research Station Schneefernerhaus (UFS) is situated at an altitude of 2653 m above sea level on the southern slope of the Zugspitze around 300 m below the mountain peak at 47.417° N and 10.977° E. Amongst other instrumentation not used in this study, it is equipped with a microwave radiometer, cloud radar, and ceilometer. These instruments are installed within a few meters of each other to assure the consistency and comparability of the measurements. The instrument specifications are summarized in Table 1. Further details on the instrumentation and retrieved datasets are provided by Kneifel et al. (2022).

Primarily, two observational and one model dataset from the Cloudnet processing chain were used to perform the data analysis for this study, namely the radar, categorize and model products (see Ewald et al. (2026)). The radar data contains variables from zenith-pointing Doppler cloud radar measurements in their original resolution depending on the instrumentation that is available at the corresponding measurement site. The radar data has a temporal resolution of 10 s (corresponding to 8425 sampled profiles for a complete day) and 488 vertical layers of 31.18 m spatial resolution each. The cloud radar data in its native resolution was used for the EDR retrieval. Typical cloud radar measurements are obtained at resolutions of 3 –

https://doi.org/10.5194/egusphere-2026-3092
Preprint. Discussion started: 18 June 2026

5 s. Therefore, the somewhat coarser temporal resolution of the radar at Schneefernerhaus may reduce the ability to resolve small-scale turbulences to some extent. However, a sensitivity analysis showed that retrieving EDR from radar data with varying temporal resolutions does not introduce a significant bias. The categorization product contains variables from different measurements (lidar, radar, microwave radiometer). All the variables in the categorization product are averaged to a common grid to simplify intercomparison between different measurement sites. The Cloudnet grid features a temporal resolution of 30 s and a vertical resolution depending on the cloud radar resolution at the measurement site (approx. 31 m for a Mira-35). The cloud radar data in the categorize product is corrected for gaseous and liquid attenuation using temperature, pressure, and humidity from model outputs and microwave radiometer measurements. The measurement and model data are used to derive a binary categorization mask, which allocates different attributes to each pixel (Hogan and O'Connor, 2004). A target classification can then be produced using CloudnetPy to identify the presence of aerosol particles, insects, or different types of hydrometeors. CloudnetPy is a Python package described in Tukiainen et al. (2020) that facilitates the processing of cloud and aerosol remote-sensing data using the Cloudnet processing scheme, as described in detail by Illingworth et al. (2007).

The specific humidity, temperature, zonal and meridional wind and pressure from the output of the European Centre for Medium Range Weather Forecasts – Integrated Forecast System (ECMWF – IFS) are used to produce the Cloudnet categorize and model products. These variables are used, e.g., to constrain the cloud phase and to ensure continuous data quality and account for effects of atmospheric parameters on the Cloudnet classification algorithm (Hogan and O'Connor, 2004). The model data is used in this study to analyze possible effects of wind shear and moisture availability on cirrus formation, and to compare the simulated cloud fraction to observations. For the analysis of the atmospheric conditions surrounding dusty cirrus events, temperature, pressure, relative humidity with respect to ice, and wind speed and direction were calculated from the provided model parameters.

Table 1. List of instruments and their specifications at the Cloudnet site Schneefernerhaus used for this study.

Instrument	Wavelength λ Frequency ν	Derived Quantities	Temporal/Vertical Res.	Vertical range
Doppler Cloud Radar METEK MIRA-35C (Hagen et al., 2022)	ν = 35.5GHz	Doppler-velocity Radar reflectivity factor Linear Depolarization Ratio	10 s / 31.18 m	300 – 15 000 m
Lidar Ceilometer Lufft CHM15k-x (Heese et al., 2010)	λ = 1064 nm	Attenuated Backscatter Volume Depolarization Ratio	30 s / 15 m	150 – 15360 m
Microwave Radiometer RPG HATPRO-G4 (Rose et al., 2005)	ν = 22–31 GHz ν = 51–58 GHz	Liquid Water Path Column Integrated Water Vapor	1 s / column	column

https://doi.org/10.5194/egusphere-2026-3092
Preprint. Discussion started: 18 June 2026

2.3 Copernicus Atmosphere Monitoring Service (CAMS) dataset

CAMS is a service provided by the Earth observation program of the European Union. For CAMS, ECMWF – IFS model output is combined with satellite and in-situ observations to create a global dataset of atmospheric parameters like air pollution, radiation, greenhouse gases, and climate forcing. A detailed description of ECMWF – IFS operational model can be found in the ECMWF Forecast User Guide by Owens and Hewson (2018).

For this study, the ECMWF Atmospheric Composition 4 (EAC4) Global Reanalysis product, a global dataset so far available for the years 2003 to 2024, was used to determine position and concentration of dust aerosol in the atmosphere and to evaluate the influence of dust on cirrus formation and structure. CAMS (EAC4) model data is freely accessible in the Atmosphere Data Store (ADS).

The CAMS reanalysis data is provided on a reduced Gaussian grid (T255) with $80\,\mathrm{km}$ horizontal resolution and 60 vertical layers extending to 0 hPa The vertical coordinate follows the model orography at surface level and gradually becomes smoother with increasing height. Variables are defined at discrete grid-point locations at the center of each grid cell and are treated as horizontally uniform within the corresponding grid cell. For Schneefernerhaus, the data were extracted at 47.41° N and 10.97° E. The geometric height of each model level was derived from the pressure at model levels. For this purpose, CAMS provides the coefficients a (pressure component independent of surface pressure) and b (terrain-following pressure component), which can be used to calculate the pressure at model level. Different parameters like aerosol composition, atmospheric chemistry, anthropogenic emissions, and biomass burning emissions are provided on 3-hourly analysis fields (Inness et al., 2019). Aerosol emission and transport is simulated using the Integrated Forecasting System – Aerosol (IFS – AER) module which considers seven different types of aerosols: desert dust, sea salt, black carbon, organic matter, sulphate, and ammonium. Desert dust aerosol is split into three separate size bins of $0.03\tilde{}0.55\,\mu\mathrm{m}, 0.55\tilde{}0.9\,\mu\mathrm{m}, \mathrm{and} 0.9\tilde{}20\,\mu\mathrm{m}$ diameter. For the emission of dust aerosol, the model accounts for the following parameters: surface winds at $10\,\mathrm{m}$, soil moisture, surface albedo in the UV to visible range, and the fraction of land not covered by vegetation, snow, or ice.

2.4 Dust load and concentration retrieval

Dust aerosol in CAMS is provided as dust mixing ratio in kg of dust per kg of air on a 3–hourly temporal resolution.

Hoose and Möhler (2012) found that super-micron (> 1 μm) dust particles are very efficient INPs and can nucleate ice at temperatures as high as -10 and saturation ratios (w.r.t. ice) of just above 1, while sub-micron (< 1 μm) dust can effectively nucleate ice below -20 and saturation ratios above 1.2. For this reason, the sum of dust mixing ratios in all three size bins was used to retrieve the total dust mixing ratio.

The total dust mixing ratio was divided by the density of air at the corresponding level to obtain the dust concentration in units of $\mathrm{g\,m^{-3}}$. The density of air ρ was calculated from pressure at model level p, gas constant of dry air R_d, and virtual Temperature T_v :

$$\rho = \frac{p}{R_\mathrm{d}} T_\mathrm{v}. \tag{1}$$

https://doi.org/10.5194/egusphere-2026-3092
Preprint. Discussion started: 18 June 2026

As the dust concentration varies greatly with height and time, a logarithmic scale was chosen for better visualization. For better comparability, a layer-integrated dust load in $\mathrm{g\,m^{-2}}$ was retrieved for each 3 hour period at which the dust concentration was provided by CAMS. The layer-integrated dust load was derived from all model levels where the temperature was below $\breve{}38$ (235 K) to assure that only dust loads at cirrus level are considered.

2.5 Eddy dissipation rate retrieval

The turbulent structure that can be observed in dusty cirrus cloud decks has been discussed by different studies (Kollath, 2010; Seifert et al., 2023). In this context, vertical air motions within clouds can be inferred from Doppler radar measurements, which provide information on vertical velocities of cloud particles. Combined with horizontal wind fields derived from numerical weather prediction models, these observations allow for the assessment of turbulence within clouds. Turbulent signatures in clouds may originate from a range of dynamical and thermodynamical processes, including gravity waves, orographic forcing, frontal dynamics, atmospheric instability driven by latent heat release during condensation or ice nucleation, sedimentation, as well as radiative-cooling-induced up- and downdrafts. However, the specific processes responsible for the turbulence observed in dusty cirrus clouds remain uncertain, and a quantitative characterization using remote sensing techniques has not yet been attempted.

An approach to quantify turbulence in the atmosphere is the EDR. The EDR represents the rate at which large scale atmospheric circulation is dissolved into thermal energy through small-scale turbulence. Griesche et al. (2020) have introduced an EDR retrieval technique using the mean Doppler-velocity, which can be integrated into the Cloudnet processing chain using CloudnetPy. This approach to derive the EDR has been used in this study to compare the magnitude of turbulence within cirrus clouds in high-dust and low-dust conditions.

Griesche et al. (2020) applied an EDR retrieval technique originally proposed by Borque et al. (2016), which assumes that turbulence is locally homogeneous and isotropic. In this case, the one-dimensional turbulent energy spectrum $S(k)$ can be defined as:

$$S(k) = a\epsilon^{\frac{2}{3}} k^{\frac{-5}{3}}. \tag{2}$$

Where $a = 0.5$ is the Kolmogorov constant, ϵ is the turbulent kinetic energy dissipation rate, and k is the wavenumber. Assuming a linear horizontal wind field, the wavenumber can be related to frequency via $k = f/V_{\mathrm{h}}$, where f is the observed frequency and V_{h} is the horizontal wind speed, and to the length scale L by $k = 2\pi/L$.

This formulation is valid within the inertial subrange, the range of scales or frequencies where energy cascades from larger to smaller eddies without external input or thermal loss. If within this range, the turbulent kinetic energy spectrum follows a $-5/3$ slope on a log-log scale (energy vs. frequency), ϵ can be determined with Eq. 3 with k_0 the intercept of the linear fit:

$$\epsilon = \left(\frac{10^{k_0}}{a^{3/2}} \right). \tag{3}$$

For the EDR calculations, continuous Doppler velocity time series of 5 minutes were used, assuming that cloud properties and wind conditions are approximately stationary during this time period. Within these 5 minutes 10% of missing data points

https://doi.org/10.5194/egusphere-2026-3092
Preprint. Discussion started: 18 June 2026

were allowed and the respective data gaps were interpolated following Chellini and Kneifel (2024). As accurately isolating the inertial subrange is essential for reliable EDR retrievals using this technique, the inertial subrange was determined by calculating a linear least squares regression of the power spectrum for 17 different wavenumber intervals. EDR was calculated for cases where the slope of the power spectrum follows a $-5/3$ slope $\pm 20\%$ following Borque et al. (2016).

EDR values for this report were calculated from model and measurement data of the Cloudnet station at Schneefernerhaus for a full year (2022) to evaluate turbulence effects o cirrus cloud cases with and without the presence of mineral dust. Radar observations at Schneefernerhaus are available at a temporal resolution of approximately 10 seconds across 488 vertical levels. To optimize computational efficiency, an EDR value was calculated every 20 seconds at each level based on the 10 second radar data, maintaining a balance between processing time and resolution. To calculate EDR exclusively at cirrus level, the Cloudnet model temperature was linearly interpolated from the standard Cloudnet grid to the increased EDR resolution.

2.6 Cloudnet model data processing

2.6.1 Relative Humidity with respect to ice

The availability of moisture seems to be a controlling factor in the formation of dusty cirrus (Griesche, 2016; Weger et al., 2018). Cloudnet provides model data of specific humidity, pressure, and temperature on the native ECMWF – IFS resolution with 137 vertical layers. To determine the influence of relative humidity on dusty cirrus formation and evaluate model outputs, relative humidity was calculated from the height-corrected Cloudnet model data. For the conversion of specific humidity to relative humidity (w.r.t. ice) RH_{ice}, several calculations had to be performed. The vapor pressure e was calculated by solving the equation for specific humidity for e with p (pressure), q (specific humidity) and 0.622 the ratio of the gas constants of dry air and water vapor (Eq. 4):

$$e = \frac{qp}{0.622 + 0.378q}. \tag{4}$$

Subsequently, saturation vapor pressure over water e_{s} (Eq. 5) and ice e_{si} (Eq. 6) were calculated using the Magnus equations, based on the model temperature T:

$$e_{\mathrm{s}} = 6.112exp\left(\frac{17.67T}{T + 243.5}\right) \tag{5}$$

and

$$e_{\mathrm{si}} = 6.112exp\left(\frac{22.46T}{T + 272.62}\right). \tag{6}$$

RH_{ice} could then be calculated for all layers and time steps from the ratio of vapor pressure to saturation vapor pressure:

$$RH_{\mathrm{ice}} = \left(\frac{e}{e_{\mathrm{si}}}\right) 100. \tag{7}$$

2.6.2 Wind speed and direction

The turbulent structure of dusty cirrus clouds has been mentioned in several studies (Kollath, 2010; Seifert et al., 2023), all of which suggest that turbulence may play a significant role in cloud formation. However, it remains unclear whether the observed

https://doi.org/10.5194/egusphere-2026-3092
Preprint. Discussion started: 18 June 2026

turbulence is caused by the presence of dust, or if it originated from other dynamic processes that subsequently contribute to the formation of the dusty cirrus cloud. To assess the potential influence of wind shear on the observed turbulence, wind speed and direction were derived from Cloudnet model data using the zonal and meridional wind components.

For calculations of wind speed and direction, the guidelines provided by the ECMWF were followed. Wind speed V was calculated from the zonal u and meridional v wind components by:

$$V = \sqrt{u^2 + v^2}. \tag{8}$$

The wind direction φ, defined as the direction from which the wind is originating, following meteorological conventions, was calculated using the $atan2$ function to properly handle all four directional quadrants:

$$\varphi = \mathrm{atan2}(-u, -v)\frac{180}{\pi}\mathrm{mod}360. \tag{9}$$

3 Results

In this section, the relationship of cirrus cloud turbulence and atmospheric dust load, based on observational and modeled data from the Schneefernerhaus station in 2022 will be investigated. The analysis focuses on variations in EDR under different dust conditions, comparing turbulent characteristics in dusty and non-dusty cirrus events. Particular emphasis is placed on processes relevant to cirrus formation.

3.1 Statistical evaluation of dusty vs. low-dust cirrus

3.1.1 Annual variability of dust load, turbulence, and cloud cover

Figure 2 shows a year-long timeline of daily mean EDR observations and daily mean dust load values. Orange bars indicate the daily mean dust load at cirrus level (in $\mathrm{g\,m^{-2}}$), while the daily mean EDR value is represented by brown horizontal bars to facilitate the identification of high- and low-EDR cases. The percentiles of EDR values are indicated by brown dashed (90th percentile) and dotted (10th percentile) lines. The blue bars denote the number of observed cirrus cloud pixels per day, normalized to the maximum observed count, illustrating the daily cloud cover as well as the relative contribution of each day to the yearly statistics. The highest dust load values in 2022 at Schneefernerhaus were observed during the summer months between, with the highest dust load on 5th June reaching $4.00 \cdot 10^{-3}\,\mathrm{g\,m^{-2}}$. This is consistent with meteorological patterns, as dust transport associated with convective processes over the Sahara occurs more frequently during this period. Although the number of distinct Saharan dust intrusions is not necessarily increased, the background dust concentration in the atmosphere tends to be elevated in summer with an average dust load of $8.97 \cdot 10^{-4}\,\mathrm{g\,m^{-2}}$ from May to August. The highest daily mean EDR values were also observed during summer with an average EDR of $1.82 \cdot 10^{-3}\,\mathrm{m^2\,s^{-3}}$ between May and August . This is unexpected as highest average wind speeds in central Europe generally occur in winter between December and February. The cirrus cloud pixel count peaks in early winter and spring, when lower air temperatures favor ice formation. The higher cloud pixel counts in spring often coincide with elevated dust load values. From the observation period, three representative cases

https://doi.org/10.5194/egusphere-2026-3092
Preprint. Discussion started: 18 June 2026

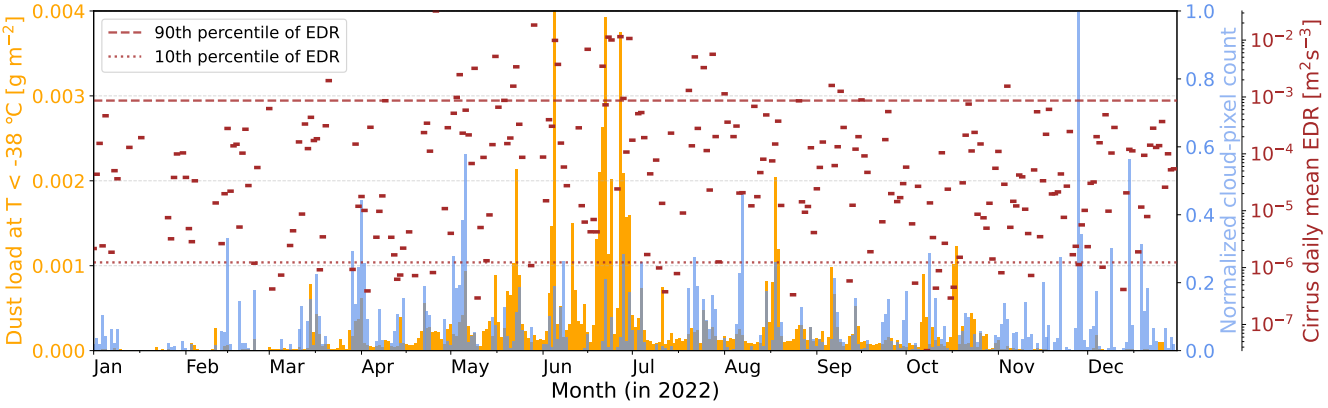

Figure 2. Daily mean dust load (orange bars), cloud pixel count (blue bars), daily mean EDR value (brown horizontal bars) at Schneefernerhaus for 2022.

of dusty cirrus cloud decks were selected for detailed analysis in section 3.2. Before presenting the case studies, a statistical analysis at 3-hour resolution is conducted to characterize the general relationship of dust and turbulence and to highlight the significance of the selected cases.

3.1.2 Turbulence of dusty cirrus vs. normal cirrus

For a direct comparison of cirrus turbulence under high and low-dust conditions, all calculated EDR values at cirrus level (temperature below $-38\,°C$) were grouped into $\pm$90-minute time windows centered at the timestamp of the modeled dust load. Scenarios with a dust load below the 10th percentile were defined as low-dust conditions, whereas scenarios with dust loads above the 90th percentile were considered high-dust conditions. In the analyzed year-long dataset, the 10th percentile dust load was $5.48 \cdot 10^{-6}\,\mathrm{g\,m^{-2}}$, while the 90th percentile was $8.91 \cdot 10^{-4}\,\mathrm{g\,m^{-2}}$. Figure 3 contrasts the distribution of EDR for all 3-hour periods with a dust load below the 10th percentile (blue, low dust load) to periods with a dust load above the 90th percentile (brown, high dust load). Both distributions were normalized by their respective maximum frequency of occurrence.

The EDR values span a wide range from $1 \cdot 10^{-10}$ to $1 \cdot 10^{-2}\,\mathrm{m^2\,s^{-3}}$ for low-dust periods and from $1 \cdot 10^{-9}$ to $1\,\mathrm{m^2\,s^{-3}}$ for high-dust periods respectively. These ranges exceed those typicalls reported in literature. However, most published EDR estimates for cirrus clouds are derived from case studies or aircraft campaigns rather than from long-term statistical analyses, which may explain the narrower ranges. Using in-situ aircraft observations of cirrus clouds obtained during several field campaigns, Quante (2006) reported EDR values between $7.00 \cdot 10^{-8}$ and $6.10 \cdot 10^{-4}\,\mathrm{m^2\,s^{-3}}$ and identified a typical range of $1 \cdot 10^{-5}$ to $1 \cdot 10^{-4}\,\mathrm{m^2\,s^{-3}}$ for the observed cirrus clouds. SComparable magnitudes were also found by \citet{turbulence_anvil_cirrus}, who compared aircraft in-situ measurements with cloud-radar-derived estimates for two anvil cirrus case studies. A clear separation of low and high dust load regimes is evident in the two distributions. The peak of each curve was calculated as the highest average bin count across 5 consecutive bins. The most frequent occurrence of EDR values in low-dust conditions was observed around $8.59 \cdot 10^{-7}\,\mathrm{m^2\,s^{-3}}$, whereas for high-dust conditions the peak is shifted by more than an order of magnitude

https://doi.org/10.5194/egusphere-2026-3092
Preprint. Discussion started: 18 June 2026

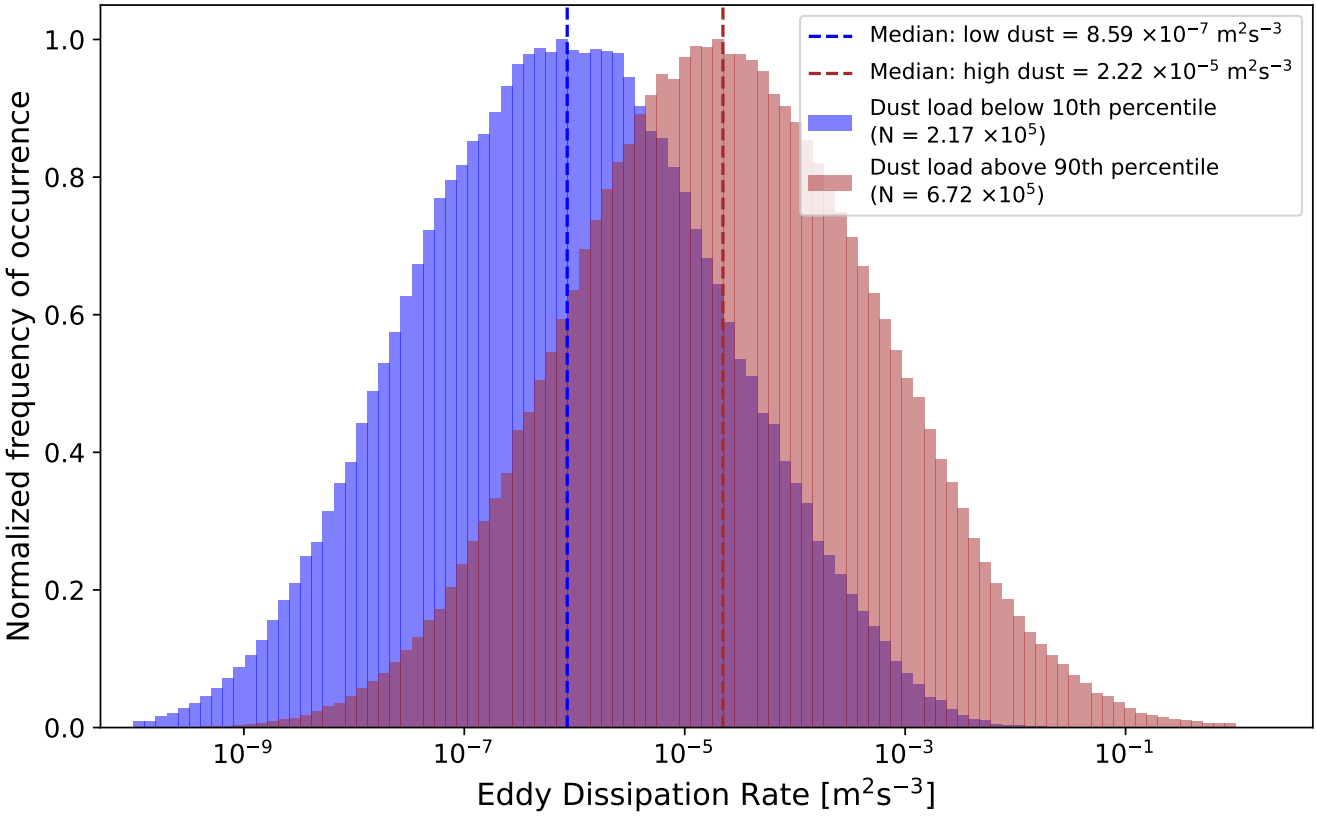

Figure 3. Logarithmic distribution of eddy dissipation rates in observed clouds for dust-free (blue) and dust-laden (brown) conditions at Schneefernerhaus in 2022. The dashed lines mark the peak of the respective distribution curve, calculated as the highest average bin-count across 5 consecutive bins.

to a value of $2.22 \cdot 10^{-5}\,\mathrm{m^2\,s^{-3}}$. The overlap of the two distributions can be attributed partly to the coarse 3 hour resolution of the CAMS reanalysis product. EDR values from each 3 hour period are assigned to one of the two distributions based on the central dust load value. This approach can lead to misclassifications in cases where the dust load is subject to strong changes over the course of the day. Ground-based lidar observations provide in principle much higher resolved dust observations under cloud free conditions. However, strong signal attenuation in lower cloud decks and masking of dust signatures in the lidar signals from cirrus altitudes hinder reliable lidar-based dust retrievals, particularly within the cirrus layer itself. Under such conditions, dust can only be detected in cloud-free regions between the cloud layers. This limitation is especially pronounced at the UFS Schneefernerhaus, as the station is frequently located within clouds (Kneifel et al., 2022).

https://doi.org/10.5194/egusphere-2026-3092
Preprint. Discussion started: 18 June 2026

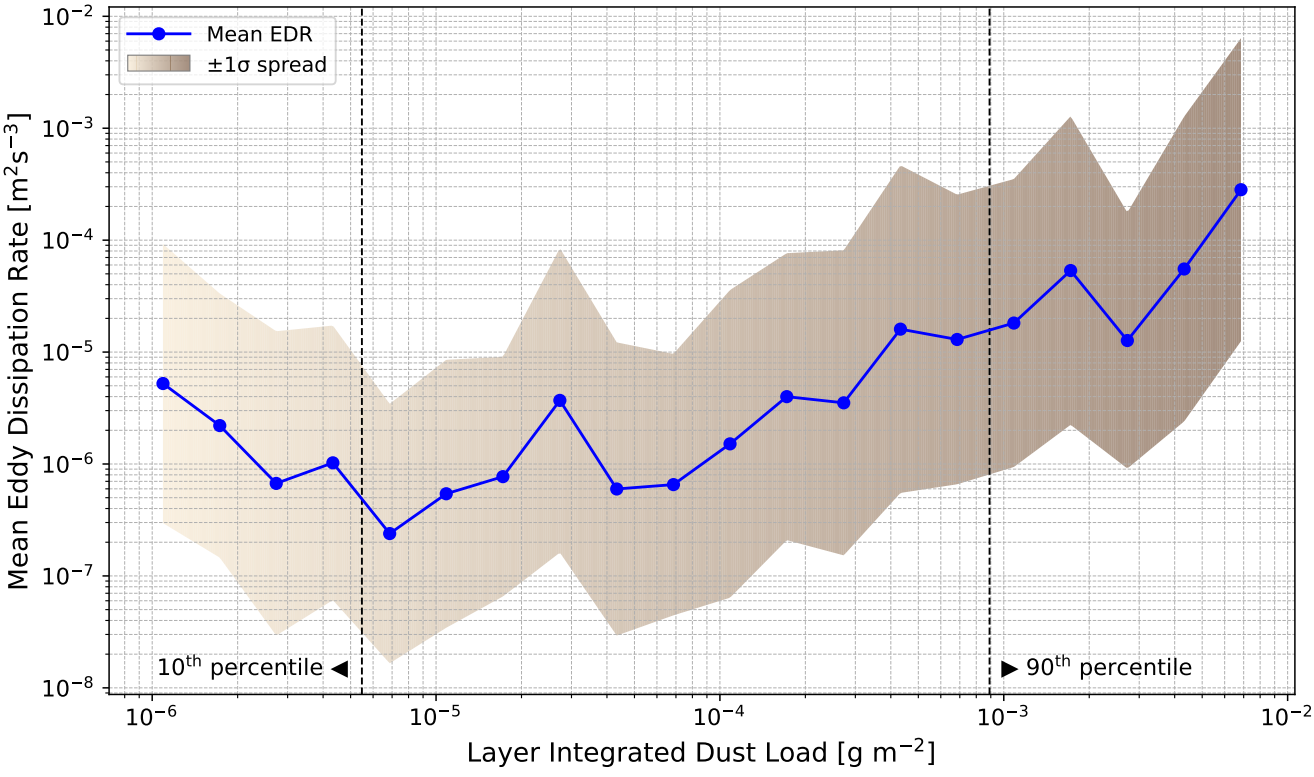

Figure 4. Log-log plot of eddy dissipation rate vs layer-integrated dust load at cirrus level. The blue dots mark the mean eddy dissipation rate of the respective dust load bin. The brown shaded area represents the $\pm 1\ \sigma$ spread of EDR values within each corresponding dust load bin, representing about 68% of observed values. The color-scale of the spread represents the increase of the dust load along the x-axis.

3.1.3 Correlation between dust load and EDR

The distribution of EDR in high and low-dust conditions illustrated in Sect. 3.1 shows that high cirrus turbulence is more likely to occur in the presence of high dust loads. However, from the simple distribution presented, it remains unclear if there is a direct correlation between the amount of dust in the atmosphere and the observed turbulence. To explore this possibility, Fig. 4 shows a direct comparison between EDR and corresponding dust load. For this analysis, mean EDR values were calculated for 20 consecutive and equally spaced dust load bins, spanning 4 orders of magnitude (5 bins per order of magnitude). Due to the coarse temporal resolution, time periods with very low cloud cover contribute equally to the correlation, despite containing substantially less information. Hence, a low-cloud pixel correction was applied by excluding time periods with a normalized cloud pixel count below 0.05 (i.e. 5 % of the maximum number of observed cloud pixel) from the evaluation.

Figure 4 shows a log-log plot with EDR on the y and the layer integrated dust load at cirrus level on the x-axis. The blue line relates cirrus turbulence to corresponding dust loads at cirrus level. The blue dots represent the mean EDR value, calculated from all EDR values within each corresponding dust bin. The $\pm\sigma$ spread of EDR around the mean is illustrated by the shaded

https://doi.org/10.5194/egusphere-2026-3092
Preprint. Discussion started: 18 June 2026

area. While no discernible trend in EDR is observed for dust loads up to $3 \cdot 10^{-5}\,\mathrm{g\,m^{-2}}$, EDR increases steadily above this threshold, reaching values that are approximately two orders of magnitude higher than those observed near the threshold. These findings indicate a strong link between cirrus turbulence and the availability of dust aerosol at cirrus level. Furthermore, scenarios with low dust load ($\leq$ 10th percentile) and high EDR value ($\geq$ 90th percentile) or high dust load ($\geq$ 90th percentile) and low EDR value ($\leq$ 10th percentile) did not occur throughout the year 2022.

3.2 Case Studies

The radar reflectivity was used to identify the location and vertical extent of the cirrus cloud layer. A dust concentration contour was added to assess the correlation between cirrus and the presence of dust. Wind speed and direction are represented by arrows of varying length and orientation to qualitatively evaluate the potential influence of wind shear (speed and directional) on cirrus formation. Relative humidity (w.r.t. ice) was included as a color contour to investigate the role of humidity in cirrus formation and to test the validity of dusty cirrus formation theories. Finally, an isoline was added at 238 K (-38 °C) to indicate the altitude above which only cirrus clouds can be observed.

3.2.1 Case 1: high dust load and high EDR – 6 May 2022

In Fig. 5, a typical dusty cirrus cloud is presented, characterized by high dust load and elevated EDR values within an extensive cirrus cloud deck. The cirrus exhibits high average dust load ($1.70 \cdot 10^{-3}\,\mathrm{g\,m^{-2}}$) and high average EDR ($9.43 \cdot 10^{-4}\,\mathrm{m^2\,s^{-3}}$) between 1:30 and 7:30 UTC, high dust load ($1.02 \cdot 10^{-3}\,\mathrm{g\,m^{-2}}$) and moderate EDR ($3.66 \cdot 10^{-4}\,\mathrm{m^2\,s^{-3}}$) from 7:30 to 10:30 UTC, and moderate dust ($5.76 \cdot 10^{-4}\,\mathrm{g\,m^{-2}}$) and moderate EDR ($1.86 \cdot 10^{-4}\,\mathrm{m^2\,s^{-3}}$) from 10:30 until 22:30 UTC (see fig. 6). The grey shaded area at heights above the 235 K isotherm (blue dashed vertical line) reveals the presence of a cirrus cloud almost throughout the whole day. This case further exhibits well developed virga below the cloud, which can be attributed to the high super saturation that was present throughout the troposphere, as well as additional ice formation in dust layers below the 235 K threshold. The observed cirrus cloud is spatially coherent with an elevated dust concentration, suggesting that cirrus formation occurs within the dust layer, which is in agreement with all cirrus clouds observed in dusty air over Cyprus as discussed by Ansmann et al. (2019). This stands in contrast to the mixing instability theory (Seifert et al., 2023), which presumes that dusty cirrus clouds form at the interface between a dry dust-laden layer and an overlying, dust-free moist air layer. Stable wind directions and significant moisture availability within the air layer of the dusty cirrus further support the in-layer formation hypothesis. A slight reduction of moisture within the observed cirrus cloud at 8 – 9 km (visible by slightly reddish colors at that height) can likely be explained by vapor deposition on the homogeneously formed cirrus ice particles simulated in the ECMWF–IFS model.

The dust concentration at cirrus level, also shown in Fig. 6, is about $5 \cdot 10^{-7}\,\mathrm{g\,m^{-3}}$. Assuming standard atmospheric conditions according to the International Standard atmosphere (ISA), the density of air at cirrus level is around $0.5\,\mathrm{kg\,m^{-2}}$. Hence, the dust concentration at cirrus level reaches a maximum of $1\,\mu\mathrm{g\,kg^{-1}}$ in the presented case. This value is much lower than the dust concentration threshold of $50\,\mu\mathrm{g\,kg^{-1}}$ used in the dusty cirrus parametrization of Seifert et al. (2023).

https://doi.org/10.5194/egusphere-2026-3092
Preprint. Discussion started: 18 June 2026

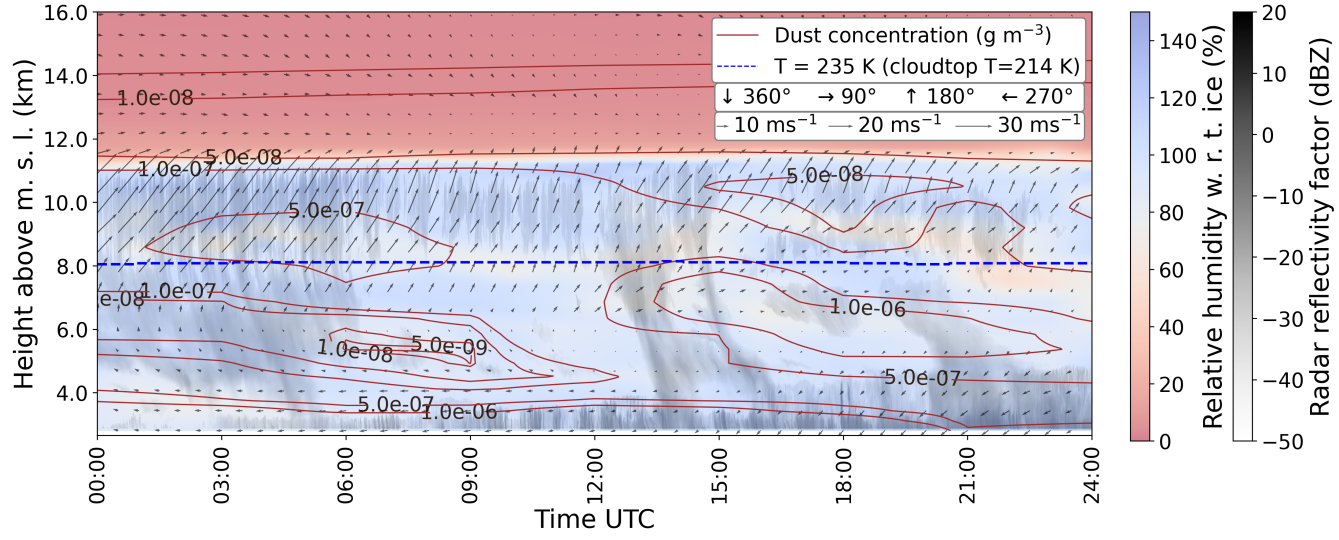

Figure 5. Time-height cross-section of measured radar reflectivity (grey color scale), relative humidity (w.r.t. ice, red and blue color scale) wind speed and direction (black arrows), and −38 °C isotherm (vertical dashed blue line) from ECMWF – IFS, and dust concentration (brown contour lines) from CAMS at Schneefernerhaus on 6 May 2022.

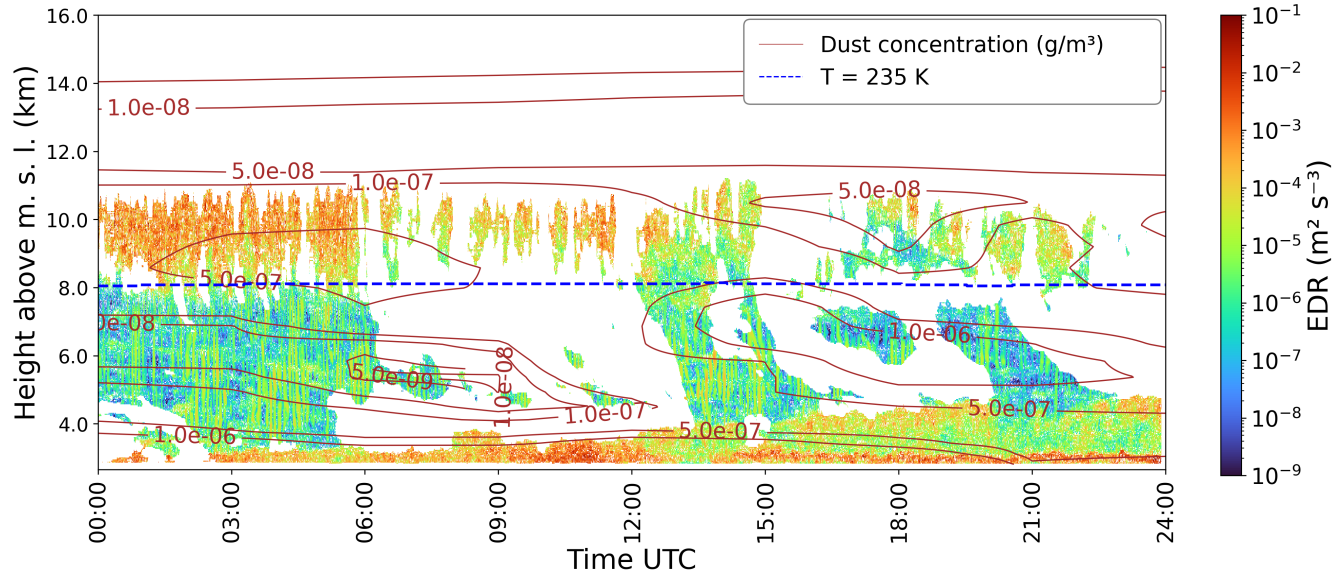

Figure 6. Time-height cross-section of EDR calculated from mean Doppler velocity and dust concentration (brown contour lines) derived from CAMS model data at Schneefernerhaus on 6 May 2022.

https://doi.org/10.5194/egusphere-2026-3092
Preprint. Discussion started: 18 June 2026

Ansmann et al. (2026) presented a method to determine the volume concentration of different aerosol types based on extinction coefficients retrieved from lidar and photometer measurements and empirical extinction-to-number and extinction-to-volume conversion factors. Dust-specific conversion factors are provided for three particle size ranges ($r > 60\mathrm{nm}, r > 100\mathrm{nm and} r > 250\mathrm{nm}$), that roughly correspond to the dust size bins employed in the CAMS simulations. Considering that sub-micron dust particles likely constitute the largest part of the simulated dust aerosol mass, dust mass concentrations simulated within the cirrus of $0.1 - 0.5\,\mu\mathrm{g\,m^{-3}}$ correspond to lidar extinction coefficients at λ= 532 nm of $Q_{\mathrm{ext532}} = 0.05 - 0.25\mathrm{Mm^{-1}}$, as well as particle number concentrations of roughly $500 - 2500\mathrm{L^{-1}}$. Assuming that all insoluble dust particles may act as INP, this corresponds to an INP reservoir of comparable size. Considering the altitude and low extinction coefficients of these dust layers, their detectability with operational lidar systems is questionable.

The nighttime radiative cooling theory is primarily based on the convective structure of dusty cirrus clouds, as observed in satellite imagery (Kollath, 2010). The convective structure is most apparent in the early morning and appears to dissipate throughout the day. However, satellite images lack vertical resolution, it is therefore possible that the enhanced visibility of the convective structure in the morning is due to shadow effects caused by the lower solar zenith angle. With an increasing solar zenith angle, these shadow effects are reduced, potentially creating the appearance that the convective structure has dissolved.

Fig. 6 shows the turbulent structure dusty cirrus case on 6 May 2022 by means of EDR. While the highest occurrence of enhanced EDR values (up to $2.63 \cdot 10^{-1}\,\mathrm{m^2\,s^{-3}}$) was observed during the night until approximately two hours after sunrise (00:00–06:00 UTC at 9000 – 11000 m), similarly elevated EDR values (up to $2.59 \cdot 10^{-1}\,\mathrm{m^2\,s^{-3}}$) were reached during the day, particularly between 10:00 and 12:00 UTC at the same altitude range. The highest average EDR values coincided with peak dust concentrations of $0.5\,\mu\mathrm{g\,m^{-3}}$. This concurrency raises the question of whether dust presence or radiative cooling plays the dominant role in generating cirrus cloud turbulence in this case. Overall, it is visible that the decrease in dust concentration over the course of the day coincides with a corresponding decrease in EDR. Additionally, the cloud cover is generally decreasing throughout the day, which makes it difficult to reach a clear conclusion. Wind shear (in direction and speed) is evident at 11500 m altitude (see 5), slighty above the cirrus top.

As Schneefernerhaus is not situated within the source region of dusty cirrus clouds, the observations mainly represent the current evolutionary stage of the cloud rather than its initial formation. However, cirrus formation is a continuous process, with ice nucleation occurring throughout the cloud lifetime. Still, mixing of a dusty and a moist air layer may have already occured prior to the observations. To evaluate this possibility, 96-hour backward trajectories were computed using the Hysplit model developed by the National Oceanic and Atmospheric Administration (NOAA). The Calculations were based on Global Forecast System (GFS) data from the National Centers for Environmental Prediction (NCEP) with a spatial resolution of 0.25° and a temporal resolution of 3 hours. Figure 7 presents the backward trajectories of two air parcels initialized at Schneefernerhaus on the 6th of May 06:00 UTC, at 11000 m (red filled circles) and 9500 m (blue filled triangles) height above sea level. Panel (a) displays the trajectories on a latitude-longitude grid, along with their respective evolution in height above sea level and relative humidity (with respect to water) in panel (b). The red trajectory represents the air mass located at the top of the cirrus cloud, where ice formation is most likely to take place. The blue line corresponds to the layer with the highest model dust concentration within the observed cloud. The trajectories reveal distinct source regions and transport pathways. The airmass at

https://doi.org/10.5194/egusphere-2026-3092
Preprint. Discussion started: 18 June 2026

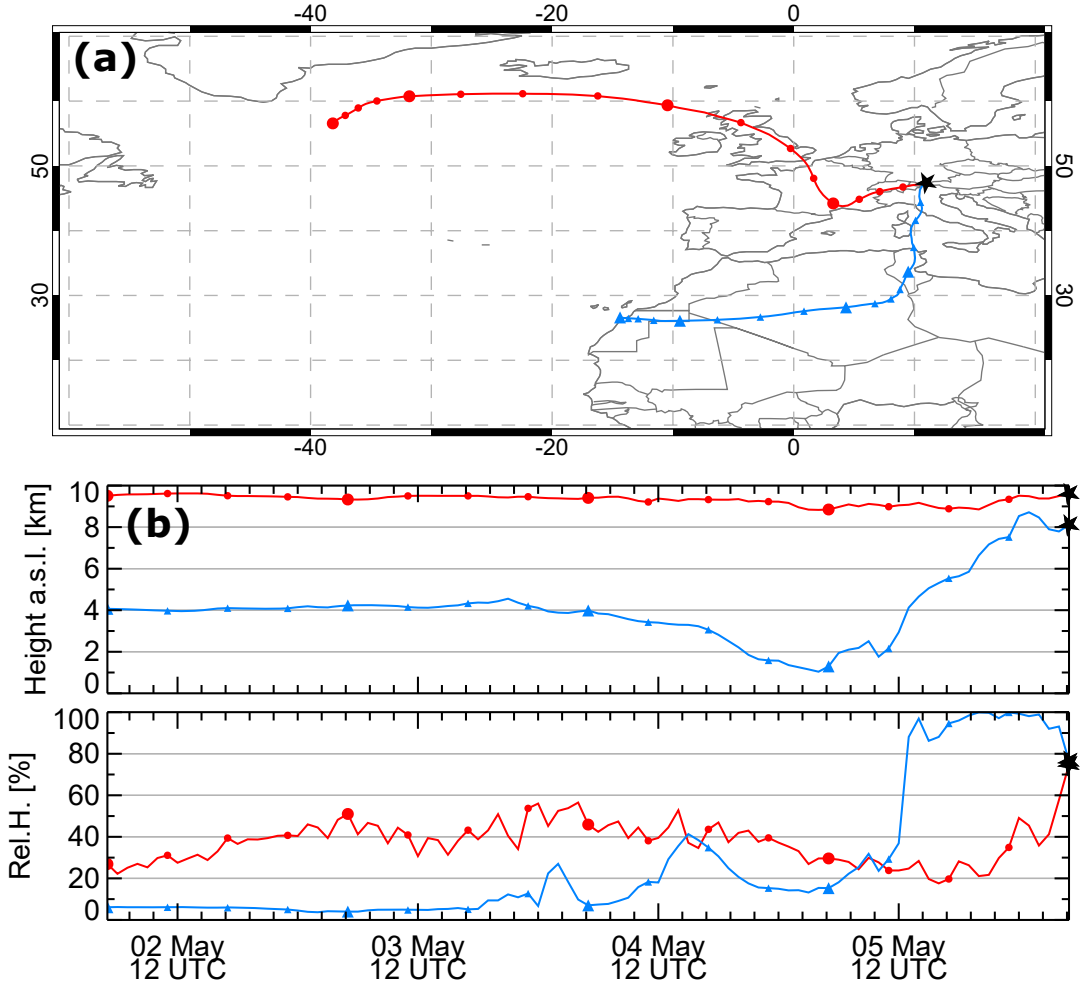

Figure 7. Hysplit 96-hour backwards trajectories of the airmass initialized on 6 May 2022 within the center of the observed dusty cirrus cloud at 9500 m (blue line) and at the top of the cloud at 11000 m (red line). Panel (a) shows the height and panel (b) the relative humidity development (with respect to water) along the trajectory based on GFS model data.

the top of the cloud originated in the North Atlantic and showed little variation inheight and relative humiditiy throughout its transport. In contrast, the dusty airmass originated from an altitude of 4 km above northern Africa just a day before reaching Schneefernerhaus, descended to boundary layer heights over the Sahara and was subsequently lifted to cirrus level. This lifting can likely be attributed to a DIBS or the warm conveyor belt. The rapid ascent is accompanied by a sharp increase in relative humidity on 5th May around 12:00 UTC. In this case, a lofting of just 2000 m is sufficient to increase the relative humidty of the Saharan air mass from 30 to 100 % , suggesting that the extreme frontal lofting associated with Saharan dust events (Fromm et al., 2016) is sufficient to reach saturation ratios necessary for heterogeneous ice nucleation, even within a dry dusty layer.

https://doi.org/10.5194/egusphere-2026-3092
Preprint. Discussion started: 18 June 2026

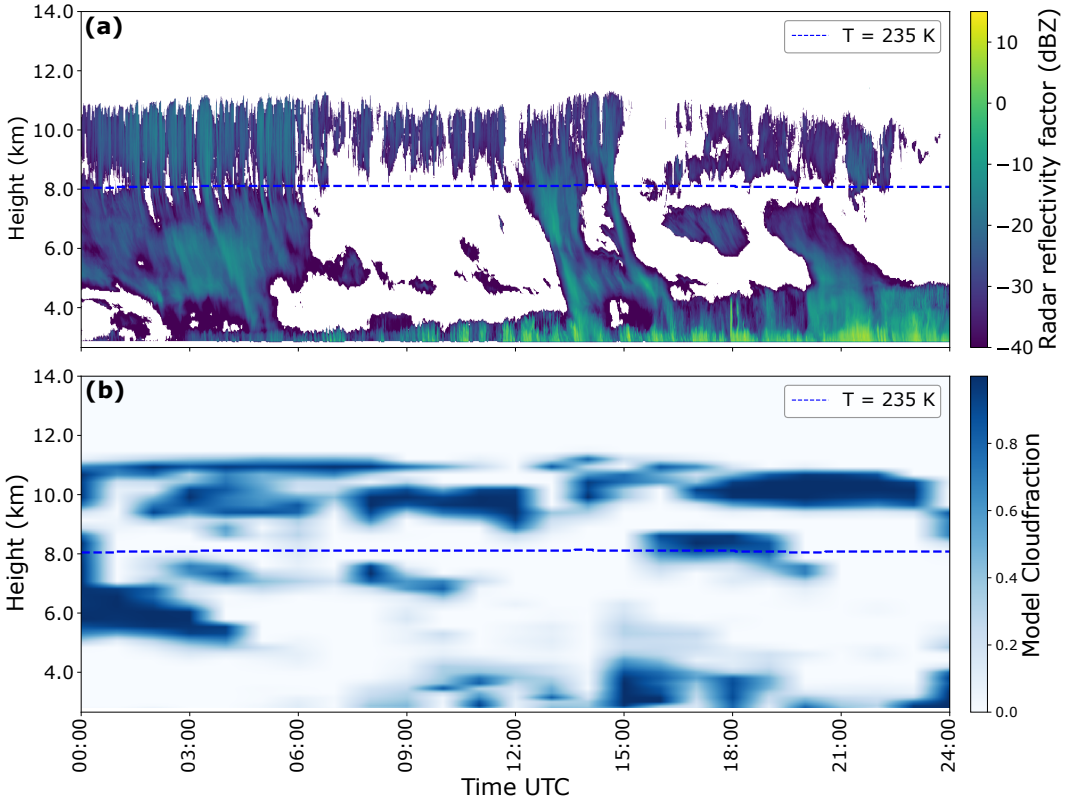

Figure 8. Time-height cross-sections of radar reflectivity (panel a) and modeled ECMWF – IFS cloud fraction (panel b) at Schneefernerhaus on 6 May 2022.

Figure 8 compares the observed radar reflectivity (panel a) with the Cloudnet model cloud fraction based on ECMWF – IFS (panel b). The radar reflectivity shows the cirrus cloud with its distinct turbulent structure between 8000 and 11000 m almost throughout the day. The modeled cloud fraction shows reasonable agreement in terms of the horizontal and vertical extent of the cirrus cloud but struggles to capture the detailed turbulent structure as well as virga and possible ice formation in the evening at 6 to 8 km altitude.

3.2.2 Case 2: High dust load and moderate EDR – 22 April 2022

In the second case study, depicted in Fig. 9, a dusty cirrus scenario with a high dust load and moderate EDR values throughout the day is examined. A cirrus cloud was observed between 01:00 and 20:00 UTC on 22 April 2022, between 8000 and 10500 m altitude. The dust load was continuously below the 90th percentile threshold, the highest encountered CAMS-simulated dust concentration within the cirrus cloud is approximately $0.1\,\mu\mathrm{g\,m^{-3}}$. However, while only moderate dust load values between 0.05 and $0.1\,\mu\mathrm{g\,m^{-3}}$ were observed within the center of the cirrus cloud layer between 01:00 and 08:00 UTC, higher dust concentrations of up to $0.5\,\mu\mathrm{g\,m^{-3}}$ were observed at the top of the cloud, where ice nucleation takes place. The comparatively

https://doi.org/10.5194/egusphere-2026-3092
Preprint. Discussion started: 18 June 2026

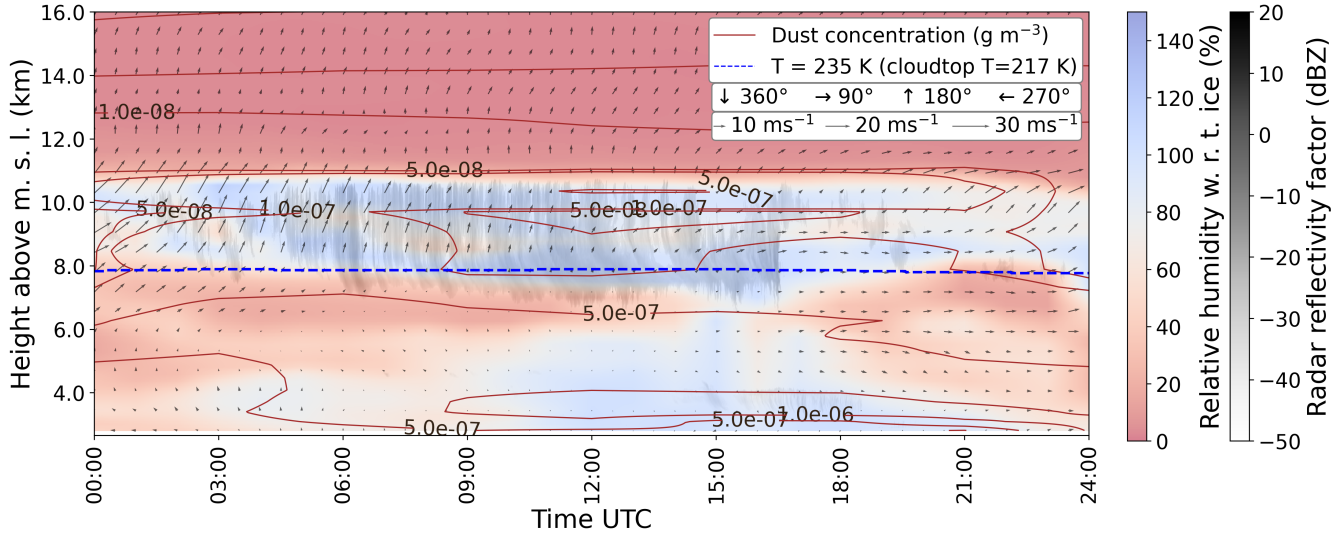

Figure 9. Same as Fig. 5 but for 22 April 2022.

low turbulence values observed at the bottom of the cirrus as shown in Fig. 11, coincided with the generally lower dust concentrations compared to the other dusty cirrus cases.

As in the previous cases, the cirrus is forming within a moist dusty air mass, with virga extending into a drier air mass below, where the ice crystals sublimate. The respective HYSPLIT back-trajectories for air parcels originating from the center (blue, 9000 m) and the top (red, 10500 m) of the cloud are shown in Fig. 10. Both pathways converge over the Sahara prior to their transport to central Europe. Notably, the dust-laden trajectory from the upper part of the cirrus cloud remains within the Saharan boundary layer for several days before being lofted. During its ascent, it crosses the lower-altitude trajectory originating from the cloud center. Both air masses undergo a pronounced increase in relative humidity during uplift over the Mediterranean (see Fig. 10).

The EDR of the presented dusty cirrus cloud on 22 April 2022 are shown in Figure 11. In this case, the highest EDR values of up to $2.54 \cdot 10^{-1}\,\mathrm{m^2\,s^{-3}}$ occurred in the morning between 04:30 and 10:00 UTC, shortly after sunrise at approximately 04:15 UTC, and are aligned with peak dust concentrations. A decrease in EDR can be observed towards the afternoon, again coinciding with a general decrease in cloud cover and dust concentration. While there seems to be a decrease of EDR in both of the observed dusty cirrus cases, more data is necessary to develop a statistical correlation and evaluate the nighttime radiative cooling theory. The effect of wind shear on the observed cirrus turbulence again seems to be negligible, as a strong deviation in wind direction or speed was not observed at cirrus altitude.

Figure 12 shows a comparison between the radar reflectivity and model cloud fraction. The dusty cirrus is rather poorly represented in the model data in this particular case. While the altitude of the simulated cloud matches well with the observed cloud at the beginning of the day, the vertical extent and cloud thickness especially after 06:00 UTC does not. Additionally, there is a notable lack of simulated cloud between 12:00 and 20:00 UTC compared to the observations.

https://doi.org/10.5194/egusphere-2026-3092
Preprint. Discussion started: 18 June 2026

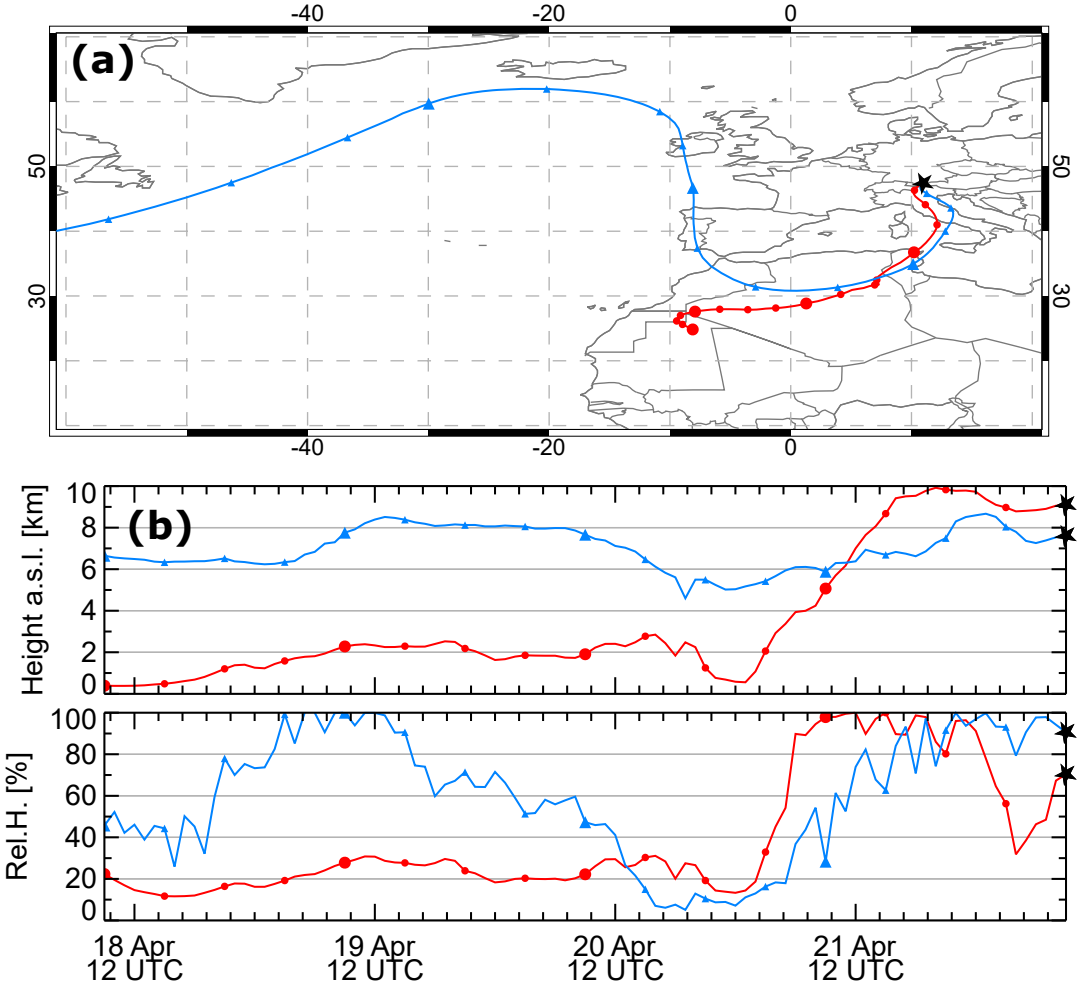

Figure 10. HYSPLIT 96-hour backwards trajectories of the airmass initialized on 22 April 2022 within the center of the observed dusty cirrus cloud at 9000 m (red) and at the top of the cloud at 10500 m (blue line). Panel (a) shows the height and panel (b) the relative humidity (with respect to water) development along the trajectory based on GFS model data.

https://doi.org/10.5194/egusphere-2026-3092
Preprint. Discussion started: 18 June 2026

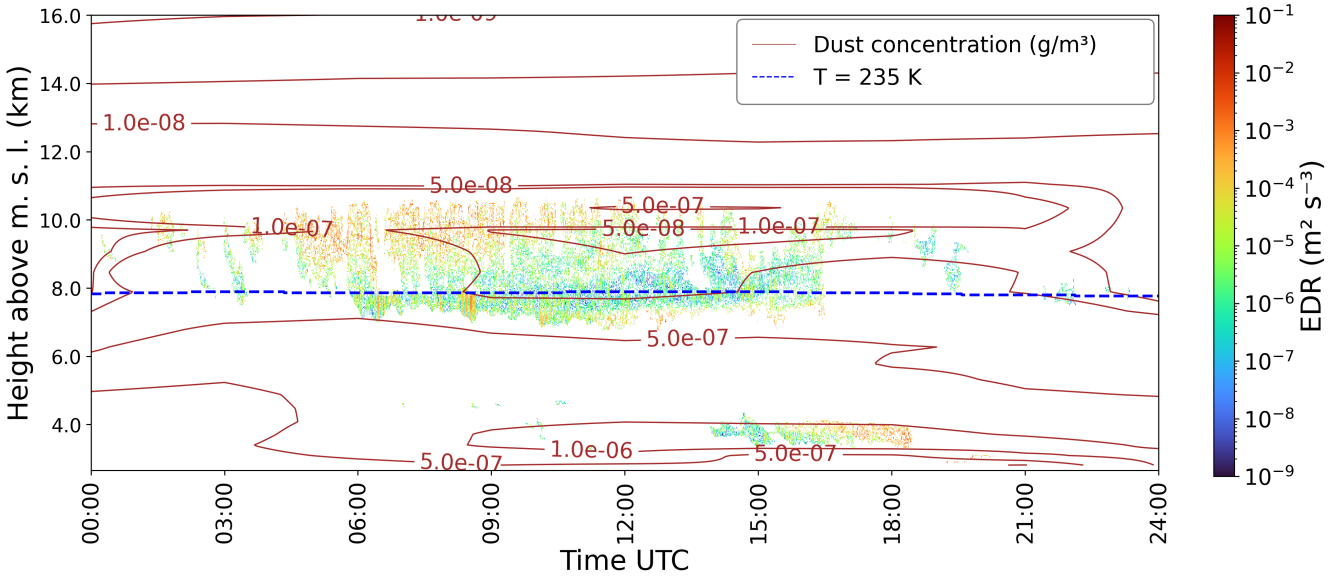

Figure 11. Same as Fig. 6 but for 22 April 2022.

In Fig. 13, the effect of the lofting of an air parcel at cirrus level on the relative humidity is simulated, following the approach of Ansmann et al. (2025b). The respective heights where the respective supersaturation threshold necessary for heterogeneous and homogeneous ice nucleation is reached are indicated by the vertical red and blue dotted lines, respectively. Panel (a) shows the ascent of an air parcel moving at a mean updraft velocity of $0.348\,\mathrm{m\,s^{-1}}$, corresponding to the mean Doppler velocity derived from cloud radar measurements at cirrus level during the analyzed period. Panel (b) shows the development of relative humidity (w.r.t. ice) and temperature as the parcel ascends at constant updraft velocity. The relative humidity w.r.t. ice was calculated using an average lapse rate derived from the model temperature profile, starting from the parcel's initial height up to 500 meters above.

The air parcel is initialized at 8005 m, a temperature of around $-38\,°\mathrm{C}$ and a relative humidity w.r.t. ice (RH) of 95 %. In this case, the threshold for heterogeneous nucleation on mineral dust aerosol of RH = 120 % (Ansmann et al. (2025b), marked by the dotted orange line), would be reached after just 175 meters of lofting or 515 seconds, respectively. In contrast, almost twice as much lifting (861 s or 300 m) would be required to reach a supersaturation of 140 %, which is considered the minimum threshold for homogeneous nucleation (Ansmann et al., 2025b; Pruppacher and Klett, 1997). Because updrafts with amplitudes of 150 m are around an order of magnitude more frequent than larger updrafts of around 300 m (Podglajen et al., 2016), heterogeneous nucleation seems to be the more plausible mechanism for cirrus formation under high dust loads. Following the onset of heterogeneous nucleation, the available supersaturation decreases. Consequently, an even greater lofting height would be required for homogeneous nucleation, making it an unlikely ice formation pathway in the observed case.

https://doi.org/10.5194/egusphere-2026-3092
Preprint. Discussion started: 18 June 2026

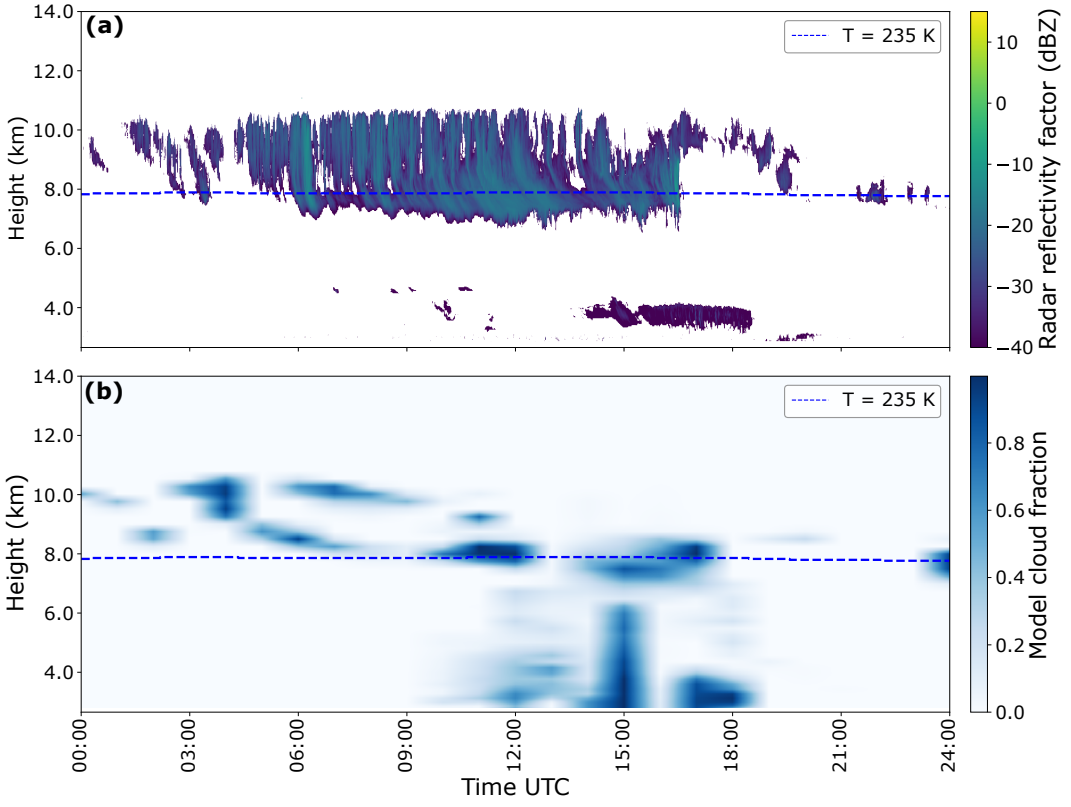

Figure 12. Same as Fig. 8 but for 22 April 2022.

3.2.3 Case 3: Moderate dust load and high EDR – 22 July 2022

The third case depicts a cloud system with moderate dust load but high EDR values observed between 14:30 and 19:30 UTC and high dust load/high EDR from 19:30 to 24:00 UTC on 22 July 2022. The structure of the cloud as well as high vertical velocities indicate a convective system. Closer inspection of Fig. 14 reveals elevated dust concentrations of 0.01 to 0.1 $\mu g\,m^{-3}$ at cirrus level, when the cloud was observed, as well as increased relative humidity. For the most part, this case does not reach the 90th percentile threshold used to define high-dust conditions. Nevertheless, it is noteworthy that all convective cloud systems with turbulent cirrus at the cloud top observed throughout 2022 also show increased dust concentrations at cirrus level. This is physically consistent, as convective processes are typically associated with high vertical velocities and therefor may entrain dust into the upper troposphere.

Despite differing from the usual dusty cirrus structure, the elevated dust concentration coincides with a peak in relative humidity (Fig. 14) and increased turbulence (see Fig. 15), similar to the 6 May 2022 case. The simultaneously observed increased humidity and turbulence together with the high dust load supports the hypothesis of in-layer formation. The distinct convective structure of the observed cloud suggests, that turbulence and relative humidity at cirrus level may be linked to

https://doi.org/10.5194/egusphere-2026-3092
Preprint. Discussion started: 18 June 2026

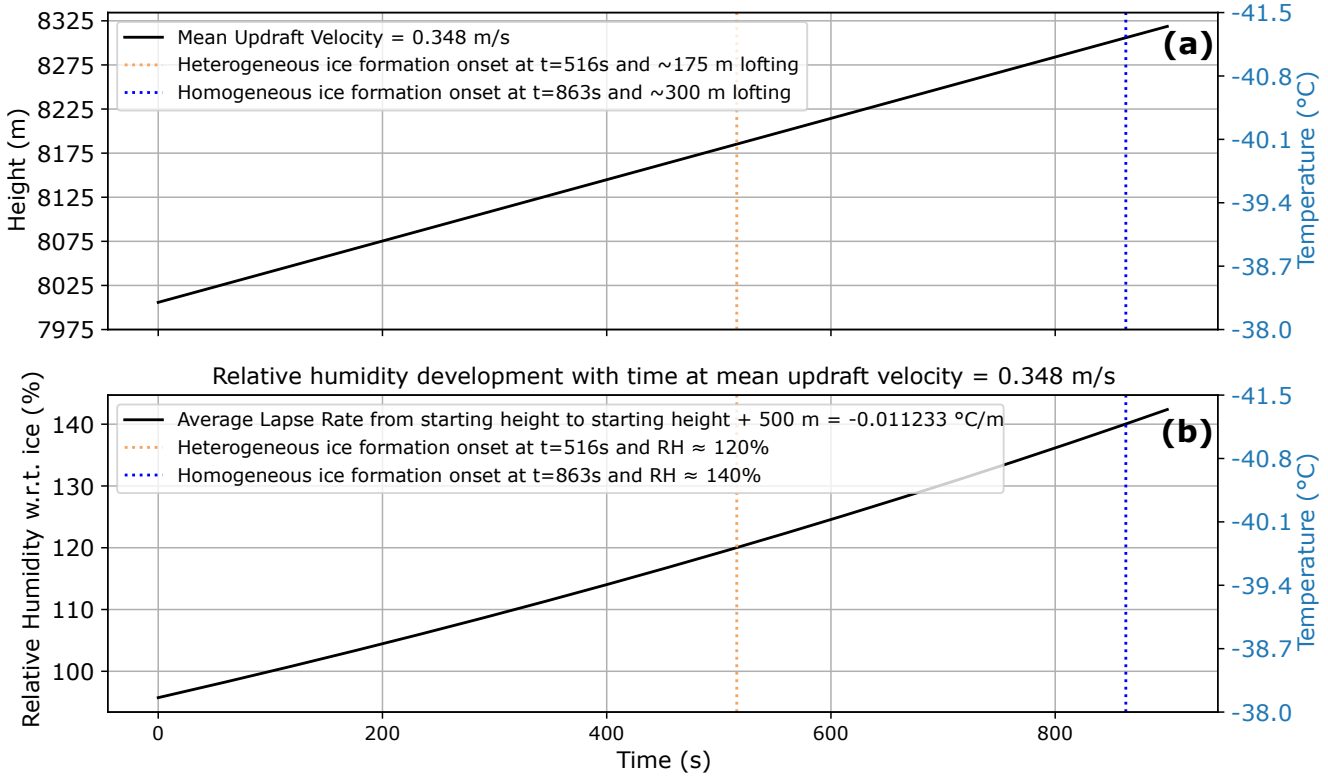

Figure 13. Lofting and relative humidity (w.r.t. ice) required for heterogeneous ice nucleation at an average updraft velocity of $0.348\,\mathrm{m\,s^{-1}}$ for the modeled cirrus gap between 14:00 and 15:00 UTC at Schneefernerhaus on 22 April 2022. Calculated from Cloudnet data.

convective processes. However, an alternative explanation is that convection transports dust from the boundary layer into the upper troposphere while simultaneously increasing relative humidity. Under these conditions the observed turbulence may serve to further promote heterogeneous nucleation, thereby contributing to the formation of the cirrus cloud.

3.3 Discussion

This section discusses the main findings presented above and their implications for dusty cirrus formation mechanisms, the role of turbulence and wind shear, and the representation of dusty cirrus in numerical weather prediction models.

Given the location of the measurement site in the German Alps, the pronounced orography could potentially influence the turbulent structure of clouds in general. However, this impact appears to be negligible, as not a single turbulent cirrus layer was identified in low-dust conditions. To assess possible orographic effects and a potential bias by general differences in the airmass transport regimes between dusty- and non-dusty conditions, HYSPLIT trajectories were calculated for each 3-hour time window during which cirrus clouds were observed (see A1). The results indicate that turbulent, high-dust scenarios (panel b) occur not only under southerly flow conditions, when air masses pass over the Alps, but also independently of airflow direction.

https://doi.org/10.5194/egusphere-2026-3092
Preprint. Discussion started: 18 June 2026

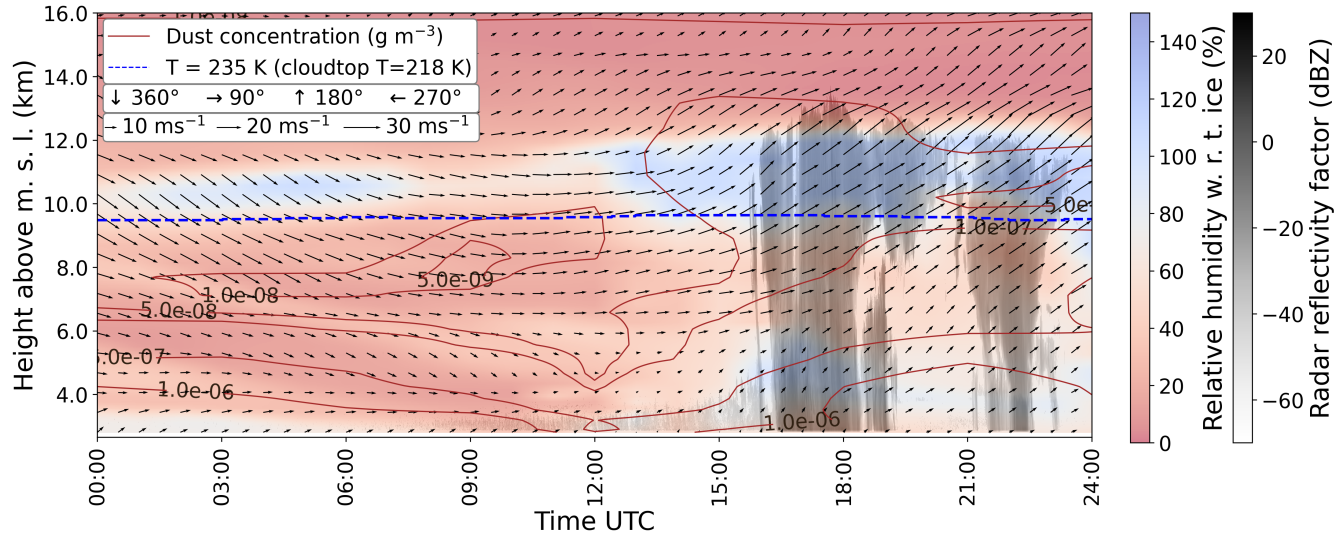

Figure 14. Same as Fig. 5 but for 22 July 2022.

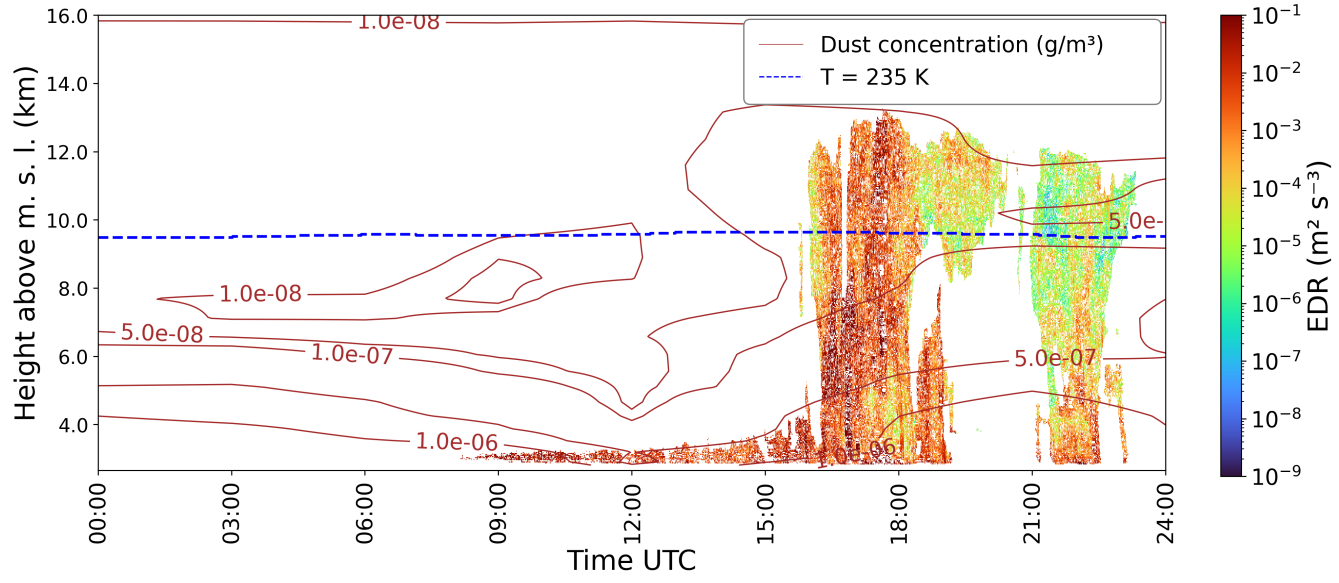

Figure 15. Same as Fig. 6 but for 22 July 2022.

https://doi.org/10.5194/egusphere-2026-3092
Preprint. Discussion started: 18 June 2026

Conversely, low-dust and low-turbulence cases (panel a) are also observed during southerly flows. Since orographically induced turbulence would be expected to occur predominantly under southerly flow conditions, these findings suggest that orography does not play a significant role in driving the observed turbulence. Throughout the year of 2022, high turbulence in cirrus clouds was only observed in presence of high dust loads. We conclude that dusty cirrus preferentially forms in dusty air-masses in which the relative humidity with respect to ice increases during sustained lofting. Because dusty air-masses have been consistently associated with enhanced turbulence, the presence of turbulent signatures appears to indicate conditions favorable for ice nucleation on dust particles. However, since turbulence could only be measured under cloudy conditions, it remains unclear if the observed cirrus turbulence is a prerequisite for ice nucleation or instead a consequence of latent heat release during ice nucleation and the resulting atmospheric instability. Observations of vertical air motions by radar wind profilers as conducted by the German Weather Service, are likely the only opportunity to investigate whether turbulence exists prior to the formation of cirrus clouds. However, such an endeavor would require a long observational dataset, since cloud-free dusty conditions are generally rare above Germany. In addition, special measurement modes would be required to track vertical air motions, as these wind profilers are typically operated to obtain horizontal wind vectors (Radenz et al., 2018).

The case studies presented in Section 3.2 investigated the relationships between various atmospheric parameters with particular focus on evaluating whether the proposed dusty cirrus formation mechanisms are consistent with state-of-the-art height-resolved observations and models. The nighttime radiative cooling theory proposed by Kollath (2010) is primarily based on the analysis of satellite images of dusty cirrus clouds, where the characteristic convective structure appears to dissipate over the course of the day. However, this pattern is not consistently supported by the radar observations presented here. In the high dust, high EDR case (6 May 2022, Sec. 3.2.1), no clear decrease in EDR values was observed during daytime. Only a slight decrease in EDR way observed just after sunrise. Instead, there was a reduction in the frequency of EDR detections, along with a general decrease in cloud cover. In another case (22 April 2022, Sec. 3.2.2), the highest EDR values occurred just after sunrise (between 04:30 and 10:00 UTC), followed by a gradual decline of cloud cover as well as EDR throughout the afternoon. In both cases, the highest density of EDR occurrence was observed in regions with the highest dust concentrations. To evaluate the validity of the nighttime radiative cooling hypothesis, a statistical analysis involving a larger sample of dusty cirrus events would be necessary. The mixing instability theory by Seifert et al. (2023) states that cirrus formation is triggered at the interface between a dry, dust-laden air layer and an overlying supersaturated, dust-free layer. However, during the three presented cases, neither the atmospheric conditions surrounding the observed cirrus clouds nor the Hysplit trajectories reveal clear evidence of such an interface. Instead, the cirrus was only observed to form within a single, supersaturated, dust-laden air mass. As a mixing instability between two air layers could not be observed, the source of the characteristic turbulence remains uncertain. Nighttime radiative cooling cannot explain similarly high turbulence values observed during night- and daytime, while the dust concentrations in the upper troposphere appear too low for purely radiative effects to be a plausible explanation for the strong observed turbulence. Although it is possible that mixing between the two layers has already completed at the time of the measurements, even very dry air masses will attain high relative humidity when lifted to cirrus levels. Therefore, it seems unlikely that the presence of an interface between a dry, dusty layer and a moist, dust-free layer is a necessary precondition for dusty cirrus formation. As shown in Figure 13, small-scale lofting alone can be sufficient to reach the supersaturation required to

https://doi.org/10.5194/egusphere-2026-3092
Preprint. Discussion started: 18 June 2026

initiate heterogeneous ice nucleation under elevated INP conditions. This is consistent with the idea that dusty cirrus formation may be initiated by small-scale lofting processes, associated with, e.g., gravity waves or wind shear, followed by the development of turbulence driven by longwave radiative cooling at the cirrus top, as proposed by Seifert et al. (2023). Atmospheric instability may also be enhanced by latent heat release during ice nucleation. The resulting turbulence may subsequently lift dusty air to altitudes where supersaturation is sufficient to trigger additional nucleation, leading to a thickening of the initial cirrus. This mechanism could explain why cirrus clouds that initially form via heterogeneous nucleation under dusty conditions often display a more turbulent structure compared to cirrus clouds that presumably form through homogeneous nucleation in low-dust environments. In contrast, homogeneous nucleation typically occurs when an air mass ascends to sufficiently high altitudes and widespread ice supersaturation is reached. This pathway is generally associated with relatively steady, large-scale lofting. Such spatially uniform cloud formation is certainly less likely to promote the development of radiatively enhanced turbulence.

The case studies further shed light on the atmospheric conditions necessary for dusty cirrus formation and the influence of wind shear on the observed turbulence. Seifert et al. (2023) proposed that vertical mixing due to wind shear or gravity waves could loft mineral dust into supersaturated layers, initiating heterogeneous ice nucleation. Their sub-grid parameterization assumes minimum thresholds of $50\,\mu\mathrm{g\,kg^{-1}}$ for dust concentration and an ice supersaturation S_i of 0.7. However, the combination of model and observational data analyzed in this study suggest that dusty cirrus clouds can already form at simulated dust concentrations of $0.5\,\mu\mathrm{g\,kg^{-1}}$. It is notable that ICON – ART indeed seems to simulate dust concentrations as high as $50\,\mu\mathrm{g\,kg^{-1}}$, while the highest dust concentrations for dusty cirrus cases simulated by CAMS were around two orders of magnitude lower. A detailed comparison of the two model configurations could help clarify the source of these discrepancies, but is beyond the scope of this study. Moreover, supersaturations in the Cloudnet model data at cirrus level generally exceed $S_i = 0.9$, which is significantly higher than the threshold used in the parameterization.

In addition, the role of wind shear as a source of turbulence within already existing cirrus clouds was investigated. Evaluating this possibility requires confidence that the observed cloud top is within the detection limit of the radar, since cloud radars may fail to detect the small ice crystals formed at the top of the cirrus due to signal attenuation. In the present study, the altitude of the measurement site where the radar is operated (around 2653 m) leads to a comparably high sensitivity at cirrus level. For one representative case on the 17th March 2022, the minimum cloud-top reflectivities ($-26\mathrm{dBZ}$ to $-35\mathrm{dBZ}$) were compared with the theoretical detection limit at 11000 m altitude. The observed reflectivity was found to be $10-20\mathrm{dBZ}$ above this threshold, indicating that the radar was capable of detecting the actual cloud top. Additional confidence is gained from the close aggreement of cloud top heights derived from ceilometer and radar observations. To gain more confidence in the evaluation, a statistical analysis of wind shear vs dust load and cirrus turbulence was performed. A bulk shear index based on Cloudnet model data was calculated as the vector difference between the mean horizontal wind vectors in layers 500 m above and below cloud top following Stull (2015). Figure 16 shows the normalized distribution of bulk shear values for low and high dust loads (panel a) as well as low and high EDR values (panel b). As the number of available bulk shear values is twice as high for dusty vs non-dusty cases, the histograms depicted in panels (a) and (b) were normalized to their respective maximum for comparability. In both panels, all distributions exhibit a pronounced peak at bulk shear values of approximately

https://doi.org/10.5194/egusphere-2026-3092
Preprint. Discussion started: 18 June 2026

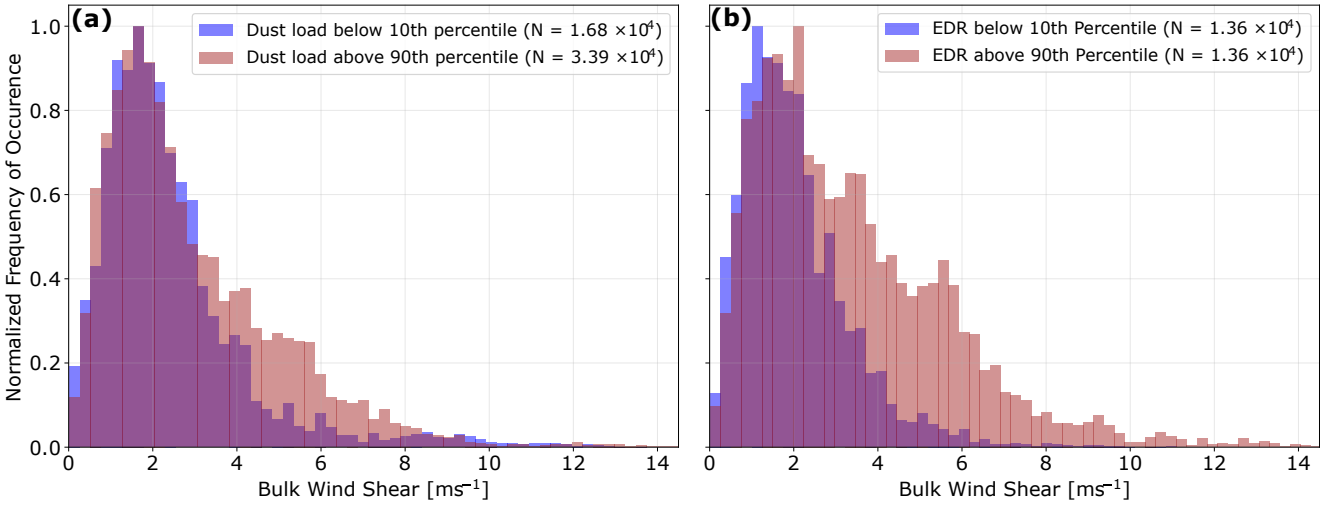

Figure 16. Distribution of bulk wind shear values for calculated for cloud top ±500 m for dusty (brown) and non-dusty (blue) cases in panel (a) as well as turbulent (brown) and non-turbulent (blue) cases in panel (b).

1.8 m s^{-1}, indicating that this value represents the most frequent occurrence for dusty and non-dusty conditions as well as for turbulent and non-turbulent cases. In panel (a), periods with high dust loads show a slight tendency toward higher bulk shear values compared with low-dust conditions. A similar shift toward somewhat larger bulk shear values is evident for turbulent cases relative to non-turbulent cases in panel (b). However, it should be noted that all turbulent cases are also associated with elevated dust loads, so the differences between the turbulent and non-turbulent distributions are not independent of the dust load. Despite a shift toward higher bulk shear, the majority of dusty and turbulent cases do not exhibit particularly strong wind shear. Moreover, some degree of correlation between EDR and bulk shear is expected, as higher shear inherently promotes the generation of atmospheric turbulence. The results therefore do not suggest wind shear to be a dominant factor in cirrus turbulence. A scatter plot illustrating the relationship between bulk shear and EDR, including the corresponding coefficient of determination (R^2 = 0.04) is provided in the appendix (Fig. A2.)

The ECMWF – IFS model, which is used for ACTRIS Cloudnet products operates with monthly mean aerosol climatologies based on CAMS reanalysis data. In the operational model, aerosol effects on cloud formation and microphysics are not considered due to their complexity. This neglects the influence of extreme dust concentrations associated with dust-infused baroclinic storms (DIBS) on cloud formation and visibility. The simulated cirrus clouds in the analyzed cases were therefore a product of homogeneous nucleation. Heterogeneous nucleation may however play a crucial role in driving cirrus formation under high-dust conditions, highlighting the need for improved ACI parameterizations. Another key limitation is the model's vertical resolution of around 300 m at cirrus level, which limits its ability to simulate small-scale processes. The difference between observed and modeled cloud fraction under dusty conditions was investigated by simulating the updraft for a case where cirrus could be observed but not simulated by the ECMWF - IFS model. The lofting required for an air parcel to reach

https://doi.org/10.5194/egusphere-2026-3092
Preprint. Discussion started: 18 June 2026

the supersaturation threshold for heterogeneous ice nucleation on mineral dust was evaluated based on the thermodynamic conditions of the respective case. The analysis demonstrated that sub-grid turbulence alone could be sufficient to initiate ice formation under the given conditions. While the vertical model resolution at cirrus height is approximately 300 m, an ascent of just 175 m would lead to sufficient supersaturation in the analyzed case. This discrepancy may partly explain why NWP models still struggle to simulate dusty cirrus clouds. Model simulations with higher resolution could help addressing this issue. It appears that vertical, rather than horizontal, resolution is the limiting factor. A vertical resolution on the order of 50 m at cirrus level may already allow for a more realistic representation of lofting-related dusty cirrus formation. While assessing the practical applicability of such an approach is beyond the scope of this study, it is worth noting that an improved representation of sub-grid cloud formation processes as discussed by Tompkins (2005) for liquid clouds, represent a promising attempt. Additionally, uncertainties in the representation of the ice nucleation efficiency of mineral dust and in distinguishing between heterogeneous and homogeneous nucleation pathways still limit the accuracy of nucleation parameterizations. A comparison of INP and ICNC values of the observed dusty cirrus cases to typical values of heterogeneously and homogeneously formed cirrus clouds would be helpful to identify the primary formation pathway. However, no suitable measurements were available for the chosen dates and location. Furthermore, convective activity appears to be poorly resolved, with thick convective clouds consistently underrepresented across the case studies, which highlights the challenge of modeling vertical air motion. This might limit the models accuracy as lofting is seen as one of the most important factors in ice nucleation (Ansmann et al., 2025a; Seifert et al., 2023; Spichtinger, 2014). Moreover, the horizontal resolution of the model may be too coarse to resolve small-scale turbulent structures, which satellite observations by Kollath (2010) indicate often occur on scales of 1 km and less. Together, these limitations highlight the need for improved sub-grid parametrization and finer resolution to accurately simulate dusty cirrus formation and associated cloud dynamics.

4 Summary and Conclusions

In the presented study, the relationship between dust, cirrus formation, and turbulence has been investigated using a combination of ground-based height-resolved remote sensing and NWP model data. For detailed information about cloud structure, turbulence, cloud cover, and atmospheric parameters (temperature, relative humidity, wind speed, and direction) a yearlong dataset from the Cloudnet station at Schneefernerhaus containing observations from radar, lidar, microwave radiometer, and ECMWF – IFS model data has been used. Dust concentrations were retrieved from the Copernicus Atmosphere Monitoring Service EAC4 Global Reanalysis product (CAMS), since lidar-derived dust properties are not available in the presence of clouds or when lower cloud decks attenuate the lidar signal. The Eddy Dissipation Rate (EDR) was calculated based on the cloud radar Doppler velocity to serve as proxy of cirrus turbulence. The layer-integrated dust load above -38 °C was used to distinguish between regular and dusty cirrus clouds. Daily mean values of dust load and EDR were calculated to produce a timeline of dusty cirrus events and to identify cases for further analysis. 3 hourly mean values for EDR as well as dust load values on a 3 hourly resolution were used to sort the observed dusty cirrus clouds into low, moderate, and high-dust as well as low, moderate, and high turbulence (low: $\leq$ 10th percentile; moderate: 10th — 90th percentile; high: $\geq$ 90th percentile).

https://doi.org/10.5194/egusphere-2026-3092
Preprint. Discussion started: 18 June 2026

Analysis of data from the reference year 2022 at Schneefernerhaus revealed no instances of turbulent cirrus clouds (EDR ≥ 90th percentile) with dust-free conditions (dust load ≤ 10th percentile). Conversely, no cases were found where dust-laden cirrus clouds (dust load ≥ 90th percentile) exhibited low turbulence (EDR ≤ 10th percentile). Combined with the clear increase in EDR at higher dust loads, these findings suggest a strong association between elevated dust levels and enhanced turbulence in cirrus clouds for cases exceeding the 90th percentile of dust load. The presence of dust in combination with enhanced turbulence creates very favorable conditions for dusty cirrus formation.

The analyzed case studies suggest, that existing dusty cirrus formation mechanisms do not fully match the observed atmospheric conditions surrounding dusty cirrus formation. They indicate, that intense lofting of dusty Saharan air masses through the warm conveyor belt (WCB) can lead to supersaturations sufficient to trigger heterogeneous nucleation on mineral dust particles. Subsequent latent heat release through ice nucleation in combination with radiative cooling at the top of the initial cirrus may promote turbulence development and cirrus thickening. Wind shear does not seem to play a significant role in driving the observed turbulence.

Comparison of the dusty cirrus observations with model results suggests that two main factors limit the accurate simulation of cirrus in the presence of dust aerosol. Firstly, monthly mean aerosol climatologies are inherently unable to reproduce heterogeneously formed cirrus cloud associated with enhanced aerosol loads. Second, the coarse vertical resolution at cirrus altitudes appears to play a critical role. In the analyzed cases, the vertical model resolution at cirrus altitude was approximately 300 m, whereas lofting of approximately 175 m was shown to be sufficient to create the conditions necessary for heterogeneous nucleation on mineral dust particles.

This study highlights the complexity of dusty cirrus cloud formation and the limitations of both observational and modeling approaches in capturing these phenomena. Below, further aspects regarding the data analysis procedure and potential future perspectives are elaborated on. The simulated dust concentrations from CAMS are available only at a relatively coarse 3-hourly temporal resolution, which complicates the precise alignment between observed clouds and simulated dust concentrations. Consequently, reliance on these simulated data introduces additional uncertainties. Nonetheless, they proved necessary given the limited availability of lidar observations at cirrus altitudes in dusty cirrus cases. Incorporation of quartz detection channels into suitable lidar systems should be considered as one possible approach to detect dust signatures within cirrus clouds (Müller et al., 2010). Additionally, an extensive search of datasets from across Europe was conducted by visual inspection of time-height cross sections of lidar profiles to identify cases in which desert dust aerosol was detectable prior to cirrus cloud formation. However, no suitable cases were found. This implies that there is strong need for a follow-up study that concentrates on identifying the formation regions of the dusty cirrus layers and the thermodynamic and aerosol conditions that prevail in these regions.

Nonetheless, the statistical analysis yielded valuable insights into the relationship between the availability of dust and cirrus turbulence. Applying the proposed methodology to additional measurement sites that provide combined lidar–radar datasets could enhance the robustness of the observed correlation and contribute to a deeper understanding of the underlying atmospheric processes. Cloudnet, with its international network of measurement sites, presents a good platform for such an extended analysis. Furthermore, information on dusty cirrus in other regions remains scarce — particularly in the outflow of

https://doi.org/10.5194/egusphere-2026-3092
Preprint. Discussion started: 18 June 2026

deserts in Central and Eastern Asia and Australia. Remote sensing data from these regions should also be evaluated to expand the understanding of dusty cirrus formation globally. Such investigations might also help to assess the potential influence of mountain ranges (i.e. the Alps) or specific synoptic conditions during Saharan dust transport events on the development of dusty cirrus clouds over central Europe. Besides Cloudnet, satellites such as EarthCARE, Calipso, or Cloudsat have the potential to provide a global view on the collocation of cirrus clouds and mineral dust or other aerosol types that can act as INP. To deepen the understanding of the relationship between dust, turbulence and cirrus formation, a synergistic analysis of these satellite observations, particularly from overpasses over ground-based remote-sensing stations, should be performed. Such an approach could provide dust and cloud properties from below and above the cirrus. In this way, the uncertainties caused by signal attenuation could be reduced. Accurate information about the dust concentration at the top of the cirrus cloud is especially valuable, because ice nucleation is most likely to initiate where temperatures are lowest and supersaturations highest. The combination of these observational datasets with model simulations of cloud coverage could further help to identify regions where aerosol-induced cirrus clouds are systematically underrepresented, potentially revealing hotspots of such effects on a global scale. Finally, long term observational datasets from the source regions of the dust would allow observations of freshly formed dusty cirrus before the airmass ages in its transit to central Europe.

Model-based dust retrievals are constrained by coarse vertical and temporal resolution, whereas height-resolved ground-based remote sensing offers significantly higher-resolution observations. However, such observations can be limited by signal attenuation in the presence of clouds. To improve the understanding of dusty cirrus cloud formation, retrievals of key microphysical properties—such as ice crystal number concentration (ICNC) and size distribution—are essential. These parameters offer critical insights into the dominant ice nucleation mechanism, as ice crystal characteristics differ significantly between homogeneous and heterogeneous nucleation. In this context, INPC–ICNC closure studies using lidar–radar synergy, such as those conducted by Ansmann et al. (2019, 2025b) or He et al. (2025) can yield valuable information on the prevailing ice formation pathways under the influence of various aerosol types, including mineral dust and wildfire smoke.

Appendix A: Backward trajectories

The HYSPLIT Offline tool was used to calculate backward trajectories for all 3-hour low- and high-dust (A1) periods during which clouds were observed. Trajectories were computed for the center of the cloud in each respective time period. To determine the cloud center, the cloud base and cloud top were first identified as the lowest and highest altitudes, respectively, at which a minimum of 10 % of the pixels were classified as cloud. The cloud center was then defined as the midpoint between cloud base and the cloud top. Panel (a) contains all trajectories of time periods with dust loads below the 10th percentile and panel (b) contaisn all trejectories of time periods with dust loads above the 90th percentile. The upper plot shows the path of the trajectories, while the lower plot relates the location of the trajectories to their respective height at that time.

https://doi.org/10.5194/egusphere-2026-3092
Preprint. Discussion started: 18 June 2026

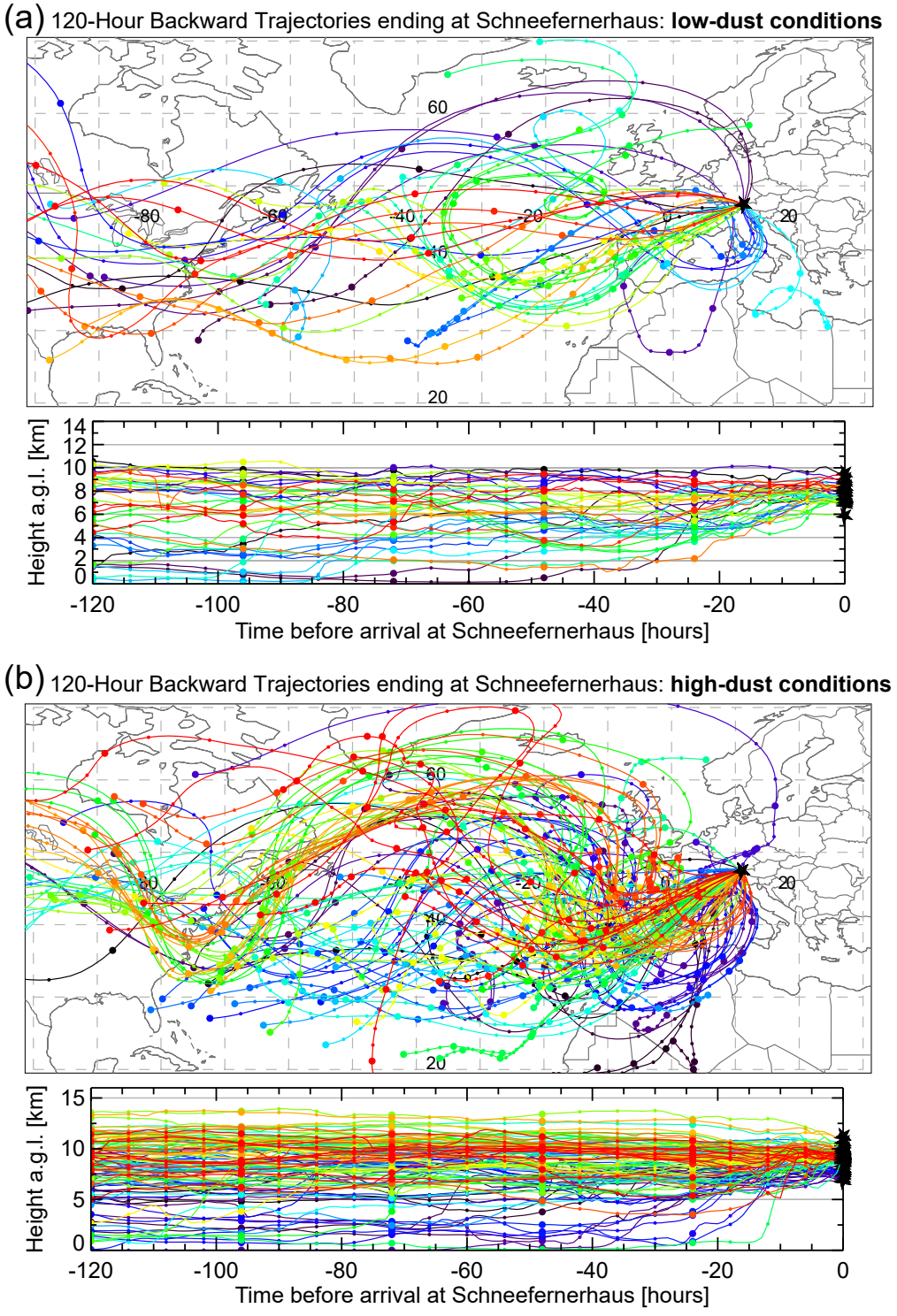

Figure A1. HYSPLIT 120-hour backward trajectories of air parcels located at the center of the cirrus cloud, calculated for each 3-hour time period with low dust loads (panel a) and high dust loads (panel b).

https://doi.org/10.5194/egusphere-2026-3092
Preprint. Discussion started: 18 June 2026

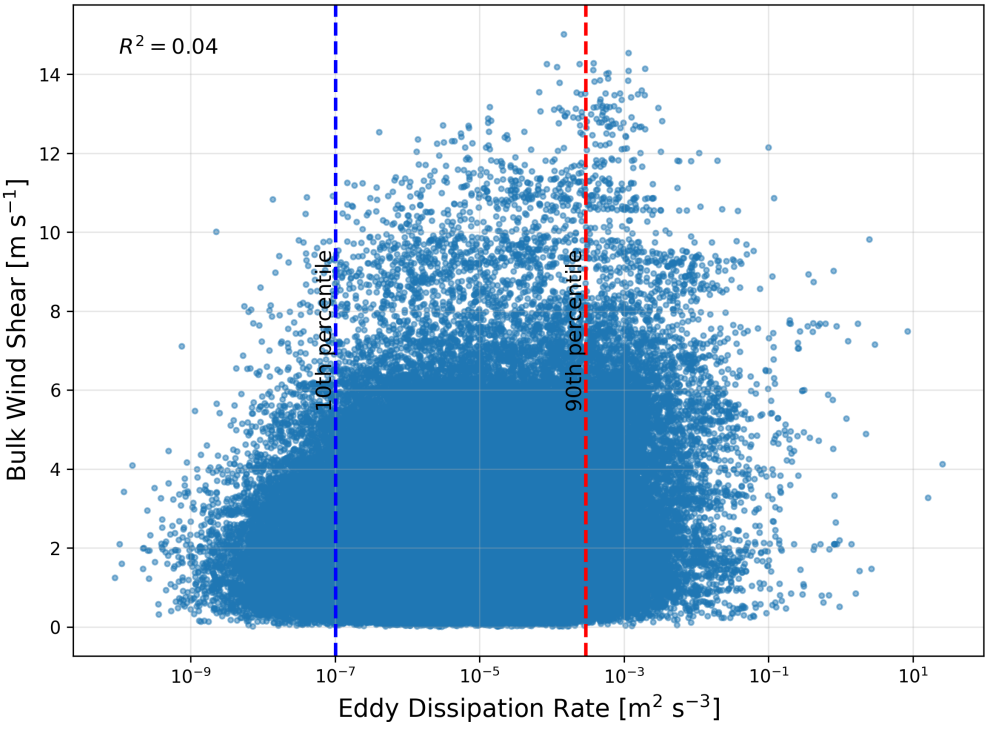

Figure A2. Scatter plot showing the correlation between bulk wind shear and eddy dissipation rate. The blue dots represent all all encountered indices of EDR and the corresponding bulk wind shear throughout the measurement period. The blue and red dashed lines indicate the 10th and 90th percentile of EDR, respectively.

Data availability. The data used in this study are generated by the Aerosol, Clouds and Trace Gases Research Infrastructure (ACTRIS) and are available from the ACTRIS Data Centre using the following link: https://doi.org/10.60656/5f9ec0d03e724afd. CAMS (EAC4) model data is freely accessible in the Atmosphere Data Store (ADS) at https://ads.atmosphere.copernicus.eu provided by the ECMWF.

Author contributions. LP conceived and designed the study and conducted the turbulence and dust-load analyses. PS, as supervisor, proposed the initial research topic and provided valuable guidance and support throughout the study. HG developed and supplied the EDR retrieval method. FE, as Principal Investigator of the cloud radar at the Environmental Research Station Schneefernerhaus, together with SK, ensured the quality of the measurement data. GMcC supported the acquisition of CAMS data. AA provided scientific guidance and proposed the lofting simulation. All co-authors contributed to the manuscript through extensive discussions and critical proofreading.

Competing interests. The correspondence author has declared that neither they nor their co-authors have any competing interests.

https://doi.org/10.5194/egusphere-2026-3092
Preprint. Discussion started: 18 June 2026

Acknowledgements. The authors thank Heike Kalesse-Los, Michael Weger, and Axel Seifert for their constructive feedback throughout this study. We are also grateful to the people responsible for operating and maintaining the measurement site at Schneefernerhaus, including staff from the German Aerospace Center (DLR), Ludwig-Maximilians-Universität München, Karlsruhe Institute for Technology (KIT), and the University of Cologne. We acknowledge ACTRIS and Finnish Meteorological Institute for providing the data set which is available for download from https://cloudnet.fmi.fi. We acknowledge ECMWF for providing IFS model data, and the Copernicus Atmosphere Monitoring Service (CAMS) for providing global atmospheric composition reanalysis data. The authors sincerely acknowledge all contributors involved in generating and maintaining these comprehensive datasets, with special thanks to Simo Tukiainen and Ewan O'Connor for their time and effort in reassessing and reprocessing the data employed in this study.

https://doi.org/10.5194/egusphere-2026-3092
Preprint. Discussion started: 18 June 2026

References

Albrecht, B. A.: Aerosols, Cloud Microphysics, and Fractional Cloudiness, Science, 245, 1227–1230, https://doi.org/10.1126/science.245.4923.1227, 1989.

Ansmann, A., Mamouri, R.-E., Bühl, J., Seifert, P., Engelmann, R., Hofer, J., Nisantzi, A., Atkinson, J. D., Kanji, Z. A., Sierau, B., Vrekoussis, M., and Sciare, J.: Ice-nucleating particle versus ice crystal number concentrationin altocumulus and cirrus layers embedded in Saharan dust:a closure study, Atmospheric Chemistry and Physics, 19, 15 087–15 115, https://doi.org/10.5194/acp-19-15087-2019, publisher: Copernicus GmbH, 2019.

Ansmann, A., Jimenez, C., Roschke, J., Bühl, J., Ohneiser, K., Engelmann, R., Radenz, M., Griesche, H., Hofer, J., Althausen, D., Knopf, D. A., Dahlke, S., Gaudek, T., Seifert, P., and Wandinger, U.: Impact of wildfire smoke on Arctic cirrus formation – Part 1: Analysis of MOSAiC 2019–2020 observations, Atmospheric Chemistry and Physics, 25, 4847–4866, https://doi.org/10.5194/acp-25-4847-2025, publisher: Copernicus GmbH, 2025a.

Ansmann, A., Jimenez, C., Knopf, D. A., Roschke, J., Bühl, J., Ohneiser, K., and Engelmann, R.: Impact of wildfire smoke on Arctic cirrus formation, part 2: simulation of MOSAiC 2019-2020 cases, https://doi.org/10.5194/egusphere-2024-2009, 2025b.

Ansmann, A., Hofer, J., Mamouri, R.-E., Haarig, M., Baars, H., and Wandinger, U.: Aerosol microphysical properties and CCN/INP information from lidar and ceilometer profiles: POLIPHON update, EGUsphere, 2026, 1–44, https://doi.org/10.5194/egusphere-2026-648, 2026.

Borque, P., Luke, E., and Kollias, P.: On the unified estimation of turbulence eddy dissipation rate using Doppler cloud radars and lidars, Journal of Geophysical Research: Atmospheres, 121, 5972–5989, https://doi.org/10.1002/2015jd024543, publisher: American Geophysical Union (AGU), 2016.

Chellini, G. and Kneifel, S.: Turbulence as a Key Driver of Ice Aggregation and Riming in Arctic Low-Level Mixed-Phase Clouds, Revealed by Long-Term Cloud Radar Observations, Geophysical Research Letters, 51, e2023GL106 599, https://doi.org/https://doi.org/10.1029/2023GL106599, e2023GL106599 2023GL106599, 2024.

Ewald, F., Mattis, I., Zinner, T., and O'Connor, E. J.: Custom collection of categorize, model, and radar data from Schneefernerhaus between 1 Jan and 31 Dec 2022, https://doi.org/10.60656/5f9ec0d03e724afd, 2026.

Frisch, S., Shupe, M., Djalalova, I., Feingold, G., and Poellot, M.: The Retrieval of Stratus Cloud Droplet Effective Radius with Cloud Radars, Journal of Atmospheric and Oceanic Technology, 19, 835 – 842, https://doi.org/10.1175/1520-0426(2002)019<0835:TROSCD>2.0.CO;2, 2002.

Fromm, M., Kablick, G., and Caffrey, P.: Dust-infused baroclinic cyclone storm clouds: The evidence, meteorology, and some implications, Geophysical Research Letters, 43, https://doi.org/10.1002/2016gl071801, publisher: American Geophysical Union (AGU), 2016.

Fusina, F. and Spichtinger, P.: Cirrus clouds triggered by radiation, a multiscale phenomenon, Atmospheric Chemistry and Physics, 10, 5179–5190, https://doi.org/10.5194/acp-10-5179-2010, publisher: Copernicus GmbH, 2010.

Griesche, H.: Evaluation of the Effect of Mineral Dust Aerosol on the Forecast Skill of Numerical Weather Prediction Models based on Remote Sensing Observations, Master's thesis, University of Leipzig, https://www.tropos.de/fileadmin/user_upload/Institut/Abteilungen/Fernerkundung/Daten_PDF/Mast-2016-Griesche-Dust_effects_on_cloud_forecast.pdf, 2016.

Griesche, H. J., Seifert, P., Ansmann, A., Baars, H., Barrientos Velasco, C., Bühl, J., Engelmann, R., Radenz, M., Zhenping, Y., and Macke, A.: Application of the shipborne remote sensing supersite OCEANET for profiling of Arctic aerosols and clouds during *Polarstern* cruise

https://doi.org/10.5194/egusphere-2026-3092
Preprint. Discussion started: 18 June 2026

PS106, Atmospheric Measurement Techniques, 13, 5335–5358, https://doi.org/10.5194/amt-13-5335-2020, publisher: Copernicus GmbH, 2020.

Hagen, M., Häring, A., Kneifel, S., and Schmidt, K.: Clouds and Precipitation Observed with Radar, in: Science at the environmental research station Schneefernerhaus / Zugspitze, pp. 79–95, Bayerisches Staatsministerium für Umwelt und Verbraucherschutz (StMUV), https://elib.dlr.de/190770/, 2022.

He, Y., Seifert, P., Jimenez, C., Radenz, M., Ansmann, A., Bühl, J., Mamouri, R., and Barja González, B.: Response of Mixed-Phase Cloud Microphysics to Aerosol Perturbations at the Contrasting Sites of Limassol, Cyprus, and Punta Arenas, Chile, Journal of Geophysical Research: Atmospheres, 130, e2024JD043 157, https://doi.org/10.1029/2024JD043157, 2025.

Heese, B., Flentje, H., Althausen, D., Ansmann, A., and Frey, S.: Ceilometer lidar comparison: backscatter coefficient retrieval and signal-to-noise ratio determination, Atmospheric Measurement Techniques, 3, 1763–1770, https://doi.org/10.5194/amt-3-1763-2010, 2010.

Hogan, R. J. and O'Connor, E. J.: Facilitating Cloud Radar and Lidar Algorithms: The Cloudnet Instrument Synergy/Target Categorization Product., https://www.met.reading.ac.uk/~swrhgnrj/publications/categorization.pdf, 2004.

Hogan, R. J., Mittermaier, M. P., and Illingworth, A. J.: The Retrieval of Ice Water Content from Radar Reflectivity Factor and Temperature and Its Use in Evaluating a Mesoscale Model, Journal of Applied Meteorology and Climatology, 45, 301 – 317, https://doi.org/10.1175/JAM2340.1, 2006.

Hoose, C. and Möhler, O.: Heterogeneous ice nucleation on atmospheric aerosols: a review of results from laboratory experiments, Atmospheric Chemistry and Physics, 12, 9817–9854, https://doi.org/10.5194/acp-12-9817-2012, publisher: Copernicus GmbH, 2012.

Illingworth, A. J., Hogan, R. J., O'Connor, E., Bouniol, D., Brooks, M. E., Delanoé, J., Donovan, D. P., Eastment, J. D., Gaussiat, N., Goddard, J. W. F., Haeffelin, M., Baltink, H. K., Krasnov, O. A., Pelon, J., Piriou, J.-M., Protat, A., Russchenberg, H. W. J., Seifert, A., Tompkins, A. M., Van Zadelhoff, G.-J., Vinit, F., Willén, U., Wilson, D. R., and Wrench, C. L.: Cloudnet, Bulletin of the American Meteorological Society, 88, 883–898, https://doi.org/10.1175/bams-88-6-883, publisher: American Meteorological Society, 2007.

Inness, A., Ades, M., Agustí-Panareda, A., Barré, J., Benedictow, A., Blechschmidt, A.-M., Dominguez, J. J., Engelen, R., Eskes, H., Flemming, J., Huijnen, V., Jones, L., Kipling, Z., Massart, S., Parrington, M., Peuch, V.-H., Razinger, M., Remy, S., Schulz, M., and Suttie, M.: The CAMS reanalysis of atmospheric composition, Atmospheric Chemistry and Physics, 19, 3515–3556, https://doi.org/10.5194/acp-19-3515-2019, publisher: Copernicus GmbH, 2019.

Intergovernmental Panel On Climate Change (IPCC): Climate Change 2021 – The Physical Science Basis: Working Group I Contribution to the Sixth Assessment Report of the Intergovernmental Panel on Climate Change, Cambridge University Press, 1 edn., ISBN 978-1-009-15789-6, https://doi.org/10.1017/9781009157896, 2023.

Kneifel, S. and Moisseev, D.: Long-Term Statistics of Riming in Nonconvective Clouds Derived from Ground-Based Doppler Cloud Radar Observations, Journal of the Atmospheric Sciences, 77, 1–47, https://doi.org/10.1175/JAS-D-20-0007.1, 2020.

Kneifel, S., Pospichal, B., Von Terzi, L., Zinner, T., Puh, M., Hagen, M., Mayer, B., Löhnert, U., and Crewell, S.: Multi-year cloud and precipitation statistics observed with remote sensors at the high-altitude Environmental Research Station Schneefernerhaus in the German Alps, Meteorologische Zeitschrift, 31, 69–86, https://doi.org/10.1127/metz/2021/1099, 2022.

Koehler, K. A., Kreidenweis, S. M., DeMott, P. J., Petters, M. D., Prenni, A. J., and Möhler, O.: Laboratory investigations of the impact of mineral dust aerosol on cold cloud formation, Atmospheric Chemistry and Physics, 10, 11 955–11 968, https://doi.org/10.5194/acp-10-11955-2010, publisher: Copernicus GmbH, 2010.

Kollath, K.: Cellular convection in cirrus clouds as a possible effect of dust aerosols, Tech. rep., EUMETSAT, https://www.eumetsat.int/media/46886, 2010.

https://doi.org/10.5194/egusphere-2026-3092
Preprint. Discussion started: 18 June 2026

Kuebbeler, M., Lohmann, U., Hendricks, J., and Kärcher, B.: Dust ice nuclei effects on cirrus clouds, Atmospheric Chemistry and Physics, 14, 3027–3046, https://doi.org/10.5194/acp-14-3027-2014, publisher: Copernicus GmbH, 2014.

Kärcher, B.: Cirrus Clouds and Their Response to Anthropogenic Activities, Current Climate Change Reports, 3, 45–57, https://doi.org/10.1007/s40641-017-0060-3, publisher: Springer Science and Business Media LLC, 2017.

Kärcher, B.: Formation and radiative forcing of contrail cirrus, Nature Communications, 9, https://doi.org/10.1038/s41467-018-04068-0, publisher: Springer Science and Business Media LLC, 2018.

Kärcher, B.: A Parameterization of Cirrus Cloud Formation: Revisiting Competing Ice Nucleation, Journal of Geophysical Research: Atmospheres, 127, e2022JD036 907, https://doi.org/https://doi.org/10.1029/2022JD036907, e2022JD036907 2022JD036907, 2022.

Kärcher, B., DeMott, P. J., Jensen, E. J., and Harrington, J. Y.: Studies on the Competition Between Homogeneous and Heterogeneous Ice Nucleation in Cirrus Formation, Journal of Geophysical Research: Atmospheres, 127, https://doi.org/10.1029/2021jd035805, publisher: American Geophysical Union (AGU), 2022.

Kärcher, B., Hoffmann, F., Podglajen, A., Hertzog, A., Pluogonven, R., Atlas, R., Corcos, M., Grabowski, W. W., and Gasparini, B.: Effects of Turbulence on Upper-Tropospheric Ice Supersaturation, Journal of the Atmospheric Sciences, 81, https://doi.org/10.1175/JAS-D-23-0217.1, 2024.

Müller, D., Mattis, I., Tatarov, B., Noh, Y. M., Shin, D. H., Shin, S. K., Lee, K. H., Kim, Y. J., and Sugimoto, N.: Mineral quartz concentration measurements of mixed mineral dust/urban haze pollution plumes over Korea with multiwavelength aerosol Raman-quartz lidar, Geophysical Research Letters, 37, https://doi.org/https://doi.org/10.1029/2010GL044633, 2010.

Owens, R. and Hewson, T.: ECMWF Forecast User Guide, https://doi.org/10.21957/M1CS7H, publisher: ECMWF, 2018.

Penner, J. E., Zhou, C., Garnier, A., and Mitchell, D. L.: Anthropogenic Aerosol Indirect Effects in Cirrus Clouds, Journal of Geophysical Research: Atmospheres, 123, 11,652–11,677, https://doi.org/https://doi.org/10.1029/2018JD029204, 2018.

Podglajen, A., Hertzog, A., Plougonven, R., and Legras, B.: Lagrangian temperature and vertical velocity fluctuations due to gravity waves in the lower stratosphere, Geophysical Research Letters, 43, 3543–3553, https://doi.org/https://doi.org/10.1002/2016GL068148, 2016.

Pruppacher, H. R. and Klett, J. D.: Microphysics of clouds and precipitation, no. 18 in Atmospheric and oceanographic sciences library, Kluwer Academic Publishers, Dordrecht, 2nd rev. and enl. ed edn., ISBN 978-0-7923-4211-3, 1997.

Quante, M.: Turbulenz in Cirruswolken mittlerer Breiten, Ph.D. thesis, Universität Hamburg, https://api.semanticscholar.org/CorpusID:129669791, 2006.

Radenz, M., Bühl, J., Lehmann, V., Görsdorf, U., and Leinweber, R.: Combining cloud radar and radar wind profiler for a value added estimate of vertical air motion and particle terminal velocity within clouds, Atmospheric Measurement Techniques, 11, 5925–5940, https://doi.org/10.5194/amt-11-5925-2018, 2018.

Rose, T., Crewell, S., Löhnert, U., and Simmer, C.: A network suitable microwave radiometer for operational monitoring of the cloudy atmosphere, Atmospheric Research, 75, 183–200, https://doi.org/10.1016/j.atmosres.2004.12.005, 2005.

Seifert, A., Bachmann, V., Filipitsch, F., Förstner, J., Grams, C. M., Hoshyaripour, G. A., Quinting, J., Rohde, A., Vogel, H., Wagner, A., and Vogel, B.: Aerosol–cloud–radiation interaction during Saharan dust episodes: the dusty cirrus puzzle, Atmospheric Chemistry and Physics, 23, 6409–6430, https://doi.org/10.5194/acp-23-6409-2023, publisher: Copernicus GmbH, 2023.

Seifert, P., Ansmann, A., Mattis, I., Wandinger, U., Tesche, M., Engelmann, R., Müller, D., Pérez, C., and Haustein, K.: Saharan dust and heterogeneous ice formation: Eleven years of cloud observations at a central European EARLINET site, Journal of Geophysical Research: Atmospheres, 115, https://doi.org/10.1029/2009jd013222, publisher: American Geophysical Union (AGU), 2010.

https://doi.org/10.5194/egusphere-2026-3092
Preprint. Discussion started: 18 June 2026

Spichtinger, P.: Shallow cirrus convection – a source for ice supersaturation, Tellus A: Dynamic Meteorology and Oceanography, 66, 19 937, https://doi.org/10.3402/tellusa.v66.19937, publisher: Stockholm University Press, 2014.

Stull, Roland B, .: Practical Meteorology: An Algebra-based Survey of Atmospheric Science, https://doi.org/http://dx.doi.org/10.14288/1.0300441, 2015.

Tompkins, A. M.: The Parametrization of Cloud Cover, Technical memorandum, Research Department, 2005.

Tukiainen, S., O'Connor, E., and Korpinen, A.: CloudnetPy: A Python package for processing cloud remote sensing data, Journal of Open Source Software, 5, 2123, https://doi.org/10.21105/joss.02123, publisher: The Open Journal, 2020.

Twomey, S.: The Influence of Pollution on the Shortwave Albedo of Clouds, Journal of the Atmospheric Sciences, 34, 1149–1152, https://doi.org/10.1175/1520-0469(1977)034<1149:TIOPOT>2.0.CO;2, 1977.

Weger, M., Heinold, B., Engler, C., Schumann, U., Seifert, A., Fößig, R., Voigt, C., Baars, H., Blahak, U., Borrmann, S., Hoose, C., Kaufmann, S., Krämer, M., Seifert, P., Senf, F., Schneider, J., and Tegen, I.: The impact of mineral dust on cloud formation during the Saharan dust event in April 2014 over Europe, Atmospheric Chemistry and Physics, 18, 17 545–17 572, https://doi.org/10.5194/acp-18-17545-2018, publisher: Copernicus GmbH, 2018.